Naval Research Reviews

Office of Naval Research
Two/1985
Vol XXXVII

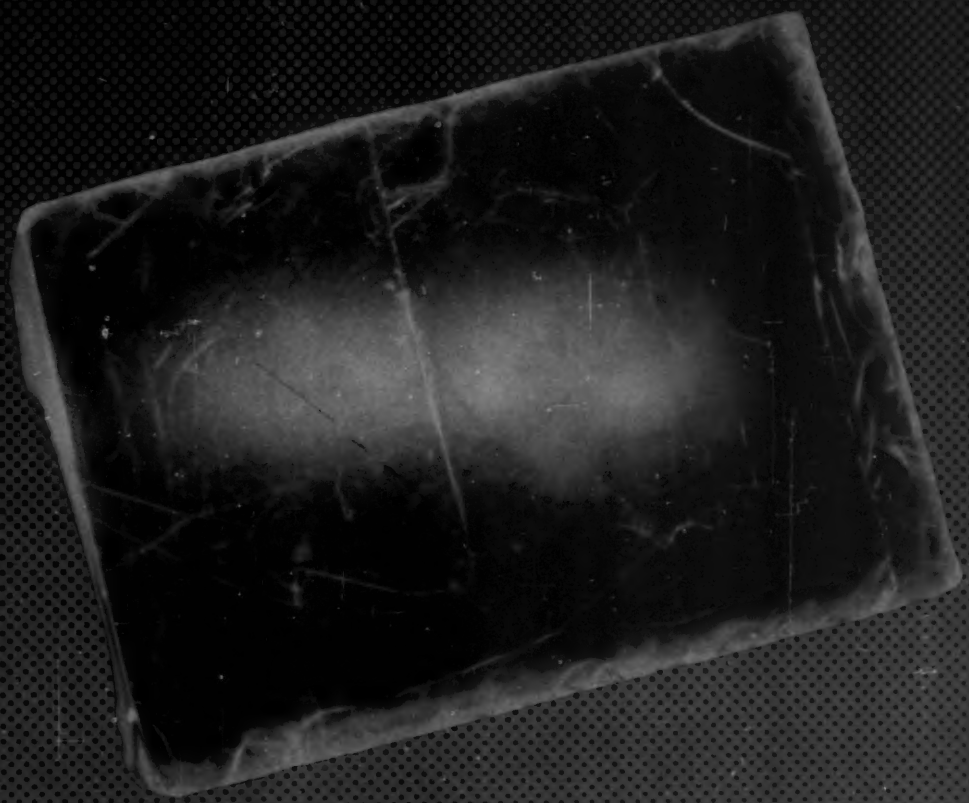

CRYSTAL OF BETA" ALUMINA

The Lithium-Thionyl Chloride Battery

The lithium-thionyl chloride battery is the highest energy density battery available commercially. The use of this battery system by the Navy is increasing because of its high power to weight and volume ratio. The discovery and early development of this battery system was supported by the Office of Naval Research in the early 1970's. The research was performed by Drs. James Auborn and Adam Heller of the GTE Laboratories. The above picture shows representative configurations of batteries and cells based on this chemistry. (Photograph courtesy of Naval Ocean Systems Center)

Naval Research Reviews

Office of Naval Research
Two/1985
Volume XXXVII

Articles

3

Battery Fundamentals: A Look Inside the Container
by Jerry J. Smith, Office of Naval Research

13

Spectroscopic Studies of Electrochemical Interfaces
by E. Yeager, B. D. Cahan, D. Scherson and M. Hanson, Case Center for Electrochemical Sciences, Case Western Reserve University

27

High Conductivity Solid Electrolytes: A Revolution in Solid State Chemistry
by Gregory C. Frarrington, University of Pennsylvania

33

Modulated Surface Vibrational Spectroscopies at Electrode/Eletrolyte Interfaces
by Stanley Pons, University of Utah, and Alan Bewick, University of Southampton, Southhampton, England

Departments

2

Introduction
by George A. Neece, Head Chemistry Division

12

Profiles in Science—
Dr. Mark S. Wrighton

2

In Memoriam
John Franklin Kincaid

About the Cover

Crystal of beta" alumina in which all of the sodium content has been replaced by Eu^{2+}. The sample is illuminated by ultraviolet light, and the Eu^{2+} is fluorescing with a characteristic yellow-green light. Nd^{3+} *beta" alumina has been shown to support both pulsed and cw laser action. Its applications as a new laser host material for* Nd^{3+} *are currently being studied.*

Naval Research Reviews publishes articles about research conducted by the laboratories and contractors of the Office of Naval Research and describes important naval experimental activities. Manuscripts submitted for publication, correspondence concerning prospective articles, and changes of address, should be directed to Code 732, Office of Naval Research, Arlington, Va. 22217-5000. Requests for subscriptions should be directed to the Superintendent of Documents, U.S. Government Printing Office, Washington, D.C. 20402. *Naval Research Reviews* is published from appropriated funds by authority of the Office of Naval Research in accordance with Navy Publications and Printing Regulations NAVSO P-35.

NAVSO P-510

Introductory Note

Electrochemistry was one of the earliest areas of physical sciences to be defined. At the beginning of this century, there were several revolutionary developments in electrode processes; but because of their inherent complexities, they defied detailed theoretical explication. After a dormant period of several decades, the field reawoke, and there was, for example, a decision by NASA to use electrochemical fuel cells for space vehicles in 1958. Accompanying the renewed interest in energy conservation which began in the late 1960's, there have been demands for new electrochemical systems for improved energy storage and conversion. These and other events, plus the availability of new experimental and theoretical techniques for studying electrochemical systems, have spurred new, exciting research in this area.

At the Office of Naval Research, a major objective of the electrochemical research program is to meet the needs of the Navy's complex weapons, propulsion, communications and sensing systems by providing the knowledge essential for the development of safe, reliable, high energy density electrochemical power sources and other applications such as high conductivity solid state sensors and opto-electronic devices.

In this special issue of Naval Research Reviews, four articles describe major areas in electrochemistry funded by ONR. Dr. Jerry Smith provides an overview of batteries to give the reader an appreciation of these rather remarkable devices and a general understanding of their behavior. Professor Ernest Yeager and his coauthors describe the research leading to the development of various spectroscopic techniques for electrochemical studies and their use. Professor Gregory Farrington presents the research on high conductivity solid electrolytes which are now being considered for a new generation of solid state sensors, high energy density storage batteries and opto-electronic devices. Professors Stanley Pons and Alan Bewick describe the reactions at the solid-liquid and solid-gas interfaces, which are controlling factors in energy-producing and catalytic devices.

For more information on the ONR electrochemical program, readers are invited to contact Dr. Jerry Smith, telephone 202-696-4409.

George A. Neece
Head Chemistry Division

In Memoriam

John Franklin Kincaid

This issue of *Naval Research Reviews* is dedicated to Dr. John F. Kincaid, well known authority on explosives and jet propulsion, assistant secretary of commerce for science and technology during the Johnson Administration, and long-time consultant and friend to the U.S. Navy. Dr. Kincaid made numerous contributions to the development and improvement of the Navy's Trident Missile System, especially in the areas of missile propulsion, detonability of high energy propellants, and the stability and life-time of electrochemical power sources. At the time of his death, he was applying his experience and expertise to issues related to the strategic defense initiative.

Dr. Kincaid's research ranged from high-pressure chemistry and rocket propulsion to laser effects. He was presented the Wyld Propulsion Award by the American Institute of Aeronautics "for outstanding achievement in the development and application of rocket propulsion systems." He also received the Naval Ordnance Development Award, and the President's Certificate of Merit for his work. He taught at the University of Rochester and was a researcher for several New York corporations before he moved to Washington, D.C. in 1958. He joined the Institute for Defense Analysis where he became director of the research and engineering support division.

In 1963, he moved to Illinois and worked for the International Minerals and Chemical Corp. He returned to Washington in 1967 to begin a two-year tour as assistant secretary of commerce. He joined the Applied Physics Laboratory of Johns Hopkins University in 1971 and was a senior scientist there when he retired in 1983.

BATTERY FUNDAMENTALS

A Look Inside the Container

By Jerry J. Smith, Office of Naval Research

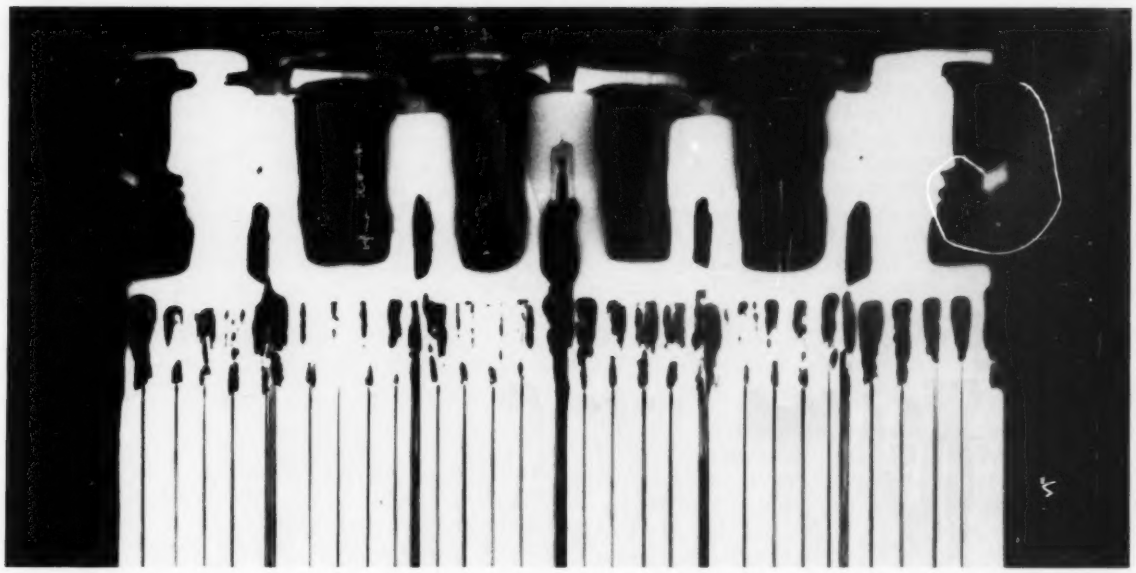

Introduction

Batteries rank near the top of any list of the most commonly used items. They are convenient, portable power sources that have permitted the development of innumerable devices of commercial and military importance. As a class, they have proven to be highly reliable; so much so that they are generally taken for granted. Energy is stored in batteries in a set of chemicals capable of reacting on demand to produce electricity. Several sets of chemicals are used so that a variety of batteries is available to the consumer.

The battery is approaching its two hundredth birthday. The first example was reported by Conte Allessandro Volta at the beginning of the nineteenth century. Volta's battery, called a pile, contained the chemical elements silver and zinc. Later in the nineteenth century, two more of the most common batteries, the dry cell and the lead-acid battery (the automotive battery), were invented. Remarkably, all three of these systems still have commercial importance.

Countless hours and financial resources have been invested in the discovery, design, development and improvement of battery systems. This investment has resulted in the development of a variety of other battery systems including nickel-cadmium and, quite recently, lithium batteries, as well as a substantial increase in the understanding of batteries and their operation. The chemical details of battery operation are complex and are even today, not well understood. Thus, battery research remains an important and necessary activity.

The U.S. Navy is a major battery consumer. Over twenty "generic" weapons, devices and equipments employ batteries for energy storage. In many cases, mission success or failure depends on proper battery performance. The Navy supports both in-house and external battery research, development, test and evaluation programs to understand and improve the performance of present battery systems and to develop new systems to meet the needs of the future.

An in-depth review of battery technology is obviously beyond the scope of this article. Here, the intent is to provide an overview of batteries to give the reader an appreciation for these rather remarkable devices and a general understanding of their behavior. Before proceeding further, the reader is encouraged to review the section labeled *Terminology* at the end of this article; the remaining text assumes a familiarity with this terminology.

Types of Batteries

Batteries can be classified in several ways, but two, by chemistry and by use, are those most often encountered in military applications. Metal-air, nickel-cadmium or lithium-thionyl chloride batteries are type descriptions based on chemistry. A more "generic" description, for example, would be "lithium batteries". This classification involves the inclusion, in one class, of all batteries that have one electrode of lithium, even though the chemistries may differ significantly.

Batteries may be used as primary batteries or as secondary batteries. The designations, primary and secondary, are unrelated to the significance or importance of the uses. Primary batteries are limited to a single discharge regardless of whether the chemistry can be reversed (recharged). Secondary batteries are used through more than one discharge/charge cycle and therefore require a chemistry which is capable of being reversed. Examples of primary batteries are the dry cell and alkaline batteries so common for flashlight and portable electronics applications. The lead-acid battery used for starting, lighting and ignition (SLI) in the automobile is an example of a secondary battery.

Other classifications of type often encountered in military applications are reserve batteries and thermal batteries. Reserve batteries are assembled and stored in an inactive state. They are activated just prior to the time that power is required. Thermal batteries are a type of reserve battery, however they are usually considered a separate group because of their special design. Reserve batteries including thermal batteries generally have long storage lives. In addition, prior to use they are not subject to unsafe conditions such as accidental short circuits. Inactive batteries are commonly constructed so that the electrolyte is stored externally and introduced to the cells in the activation process. Power may then be drawn from the battery. In thermal batteries, the electrolyte is solid and essentially non-conductive at the storage temperature. Activation is achieved by rapid heating of the battery to melt the electrolyte and make it conductive. Present thermal batteries operate at temperatures around 400 °C. As a result of these high temperatures and the accompanying high chemical reaction rates, thermal batteries provide relatively high powers for short periods of time (a few minutes). These batteries are usually constructed with a pyrotechnic material as a part of the internal components. Ignition of the pyrotechnic can produce activation times of less than one second.

Battery Properties

All batteries exhibit certain properties in common. All are composed of one or more units called cells each containing two electrodes and an electrolyte. The two electrodes, the anode and cathode, may be solids, liquids, gases or a mix, e.g., one solid and one liquid. The electrolyte is normally liquid, although batteries containing solid electrolytes are becoming more common. The electrolyte must be an ionically conducting material. Proper operation requires that one or more of the chemical species associated with the electrochemical reaction be mobile in the electrolyte.

Most batteries, particularly those containing liquid electrolytes, also contain a separator. Separators often are mats of fiberglass or paper-like materials. Their primary purpose is to prevent short circuits due to electrical contact between the two electrodes. Separators also retain electrolyte in the region between the electrodes. Research now underway may lead to separators that play an active role in battery operation by influencing the direction and rate of ion flow in the cells.

The open-circuit voltage is the voltage or potential in volts which a battery produces when no external connection between the electrodes is made. This potential depends on thermodynamics so that a specific electrochemical reaction will produce a potential that is relatively fixed. Cell voltage is related to free energy through the Nernst equation (Equation 1),

$$E^\circ = \frac{-\Delta G^\circ}{nF} \qquad (1)$$

in which E° is the standard potential, ΔG° is the standard free energy for the electrochemical reaction, n is the number of electrons involved in the reaction and F is the Faraday constant (about 96,500 coulombs). At conditions other than standard conditions of temperature (25 °C) and concentrations (1 molar), the cell potential can be calculated from the equation,

$$E = E^\circ - \frac{RT}{nF} \ln Q \qquad (2)$$

where R is the gas constant, T is the temperature and Q is the concentration quotient (product concentrations over reactant cooncentrations) for the cell reaction.

The working voltage of a battery is less than its open circuit voltage. This difference is the polarization. The magnitude of the polarization depends on factors that include chemical composition, temperature and rate of discharge. Polarization results from internal cell resistances, concentration gradients produced during reaction, and activation effects that depend on the electrode and the specific chemical reaction involved. Much effort has been devoted to undertanding the causes of polarization and to the development of catalysts to reduce its magnitude. Polarization produces inefficiencies in batteries that in turn produce heat and reduce the energy and power density.

Batteries are designed for specific applications rather than as general power sources. Certainly some batteries function satisfactorily in multiple uses, but most

batteries are not interchangable from one application to another without some degradation of performance. Comparison of different batteries, even of the same chemistry, must be done carefully. This is particularly true for batteries for military applications. Requirements vary widely in terms of rates, energy and power density, temperature of operation, load profiles and duty cycles so that two batteries of the same size and chemistry may vary considerably internally and behave quite differently. Electrode size, shape and porosity, separator thickness and composition, and electrolyte composition may all differ. This uniqueness requires that battery design be an important part of the development of the systems which contain them.

Battery Construction

Batteries are designed to provide power to some external circuit at a particular voltage and current for a length of time determined by their capacity. In assembling batteries, cells have the positive terminal of one cell connected to the negative terminal of the next cell. The result is a battery whose voltage is the sum of the individual cell voltages; each cell carries the same and total battery current. Parallel connection means the individual cells have their terminals of the same polarity connected. Parallel cells produce a battery whose voltage is that of the cell, but whose current is now the sum of individual cell currents. Parallel connection effectively increases the electrode surface area. Many batteries include both series and parallel connected cells to produce both a high battery voltage and a high current capability.

Figures 1a.-1e. show typical construction details for several different battery configurations. Figure 1a is a schematic of the "button" or bobbin cell. This style of battery is usually of single cell construction. Several different chemistries are used. These batteries are used to power devices that operate at low powers, such as watches, hearing aids, and other small electronic devices.

Figure 1a

Construction details for the battery configuration known as the "button" cell.

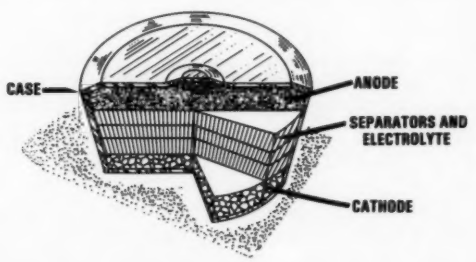

Figure 1b

Typical alkaline "D" cell construction.

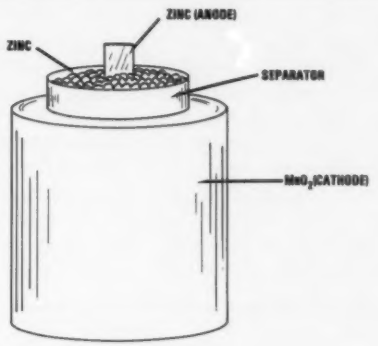

Figure 1c

Spiral wound, "jelly roll," design.

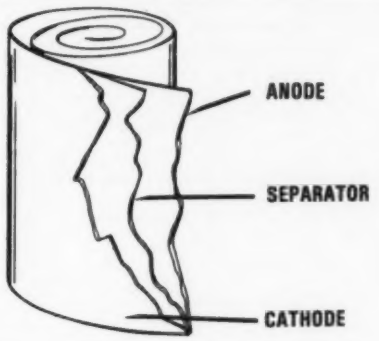

Figure 1b illustrates the general construction of the familiar alkaline battery, e.g., the C or D cell used in flashlights and portable radios, etc. The anode is high surface area zinc with a zinc metal strip connecting tab. The zinc is slurried with an aqueous potassium hydroxide electrolyte. The cathode is manganese dioxide pressed into a hollow cylinder. The separator is placed between the zinc slurry and the manganese dioxide cathode.

Figure 1c shows a type of construction that optimizes the total electrode area. In this construction the electrodes and separator are fabricated as long sheets of the appropriate material, stacked, then rolled into the final cylindrical configuration. This construction is also called spiral wound.

A schematic of the bipolar plate configuration is given in Figure 1d. This configuration is used in batteries that are designed to operate at high rates and short times.

The construction minimizes the number of internal nonactive components. Individual cells are connected by the back to back stacking arrangement. The substrate, often nickel, serves both the cathode of one cell and the anode of the adjacent cell. This arrangement puts the cells in series. Each group of series-connected cells are separated from the next by an insulating partition. One disadvantage of this construction is the presence of shunt currents. Each cell shares a common electrolyte volume with the others in the same series connected group. Each electrode therefore "sees" all of the others, that is any anode can discharge against any other cathode. While the discharge within a given cell dominates, a fraction of the current flows to the other cells. This results in an inefficiency, through a continuous loss in capacity.

Figure 1d

Bipolar plate design.

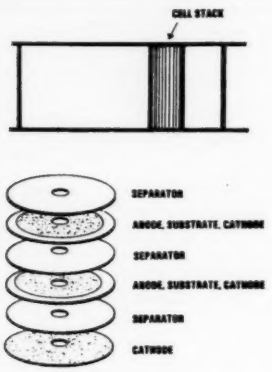

Figure 1e

Thermal battery.

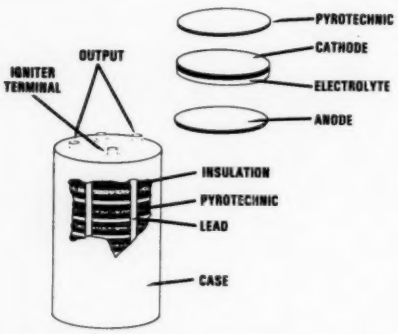

Nonetheless, this configuration is the one of choice for high rate, high energy density batteries such as those for torpedo propulsion.

The construction of a typical thermal battery is shown in Figure 1e. This construction resembles other stacked electrode configurations except for the presence of the pyrotechnic activator and the insulation for thermal control.

All of these configurations result from applying certain design goals to achieve a set of specific battery properties. These properties are summarized in Table 1. The electrical energy that a battery is capable of delivering is roughly proportional to the cell voltage; therefore, maximizing the cell voltage contributes to a maximization of the battery's energy. Because the voltage is determined primarily by the cell chemistry, it is one of the earliest properties to be fixed.

Maximizing the number of electrons in the cell reaction yields the maximum current for a given set of conditions and minimizes the amount of reactants necessary to produce a given amount of capacity. The number of electrons per reaction is also determined by the cell chemistry.

Use of the lightest possible reactants produces the maximum energy density for a given battery design. This objective is one of the factors to be considered in choosing the cell chemistry.

Fast reaction rates are necessary to sustain battery performance over a range of rates. This factor contributes to the power density.

Table 1

Battery Design Goals
Maximum Cell Voltage
Maximum Number Of Electrons In Cell Reaction
Lightest Possible Reactants
Fast Reaction Rates
High Electrolyte Conductivity
Insoluble Reactants
Minimum Construction Materials

The electrolyte provides the current path within the cell to complete the circuit. The current through the electrolyte is carried by ions. High electrolyte conductivity minimizes the internal cell resistance which in turn reduces polarization, heat generation, and limiting currents.

Normally it is important to construct batteries of electrode materials that are insoluble. This ensures that the reactants are not present in the electrolyte in a concentration high enough to react at open circuit. Such a

reaction would cause the reactants to be depleted through unproductive reaction, a process called self-discharge, during storage or as a parasitic reaction during discharge and would lead to a short battery lifetime. There are battery systems available today in which one of the reactants is a liquid in direct contact with the other which is a solid, e.g., lithium-thionyl chloride batteries. Self discharge does not occur in this system because the thionyl chloride reacts initially with the lithium to form a passivating film of lithium chloride.

Finally, minimum use of construction materials is necessary to maximize the energy density of the cell. Only the active materials contribute to power production. Any materials used in the case, tabs, or insulation will increase the weight and volume without increasing the energy.

Measures of Performance

Energy and power density are measures of battery performance. High energy and power density batteries are capable of delivering larger amounts of energy at higher rates than batteries of lower densities. Given the battery size and weight, the higher the specific energy and power the higher the output energy and power; or for a given amount of energy and/or power, the battery with the highest specific power and energy will be smallest and lightest.

Energy density (specific energy) can be calculated from the battery voltage, E, capacity, C and weight, W, using Equation 3

$$\text{Energy Density} = \frac{E \times C}{W}. \qquad (3)$$

Likewise, the power density can be calculated from Equation 4, where I is the current,

$$\text{Power Density} = \frac{E \times I}{W}. \qquad (4)$$

The energy density is normally given in units of watt-hours per kilogram and the power density as watts per kilogram. The respective volumetric energy and power densities can be calculated using the same equations but substituting battery volume, usually in liters, for battery weight. Energy density is a quantity which can be calculated easily for most actual and projected systems. Power density, on the other hand, depends on design and use; it is difficult to estimate accurately before a battery is constructed. It is best determined from a battery's performance.

The theoretical energy density for a particular electrochemical reaction (not including grids, tabs, separator, case, cover, or terminals) can be calculated from Equation 5,

$$\text{Energy Density} = \frac{2.68 \times 10^4 \, n \times E}{M}, \qquad (5)$$

where n is the number of electrons associated with the electrochemical reaction and M is the sum of the atomic/molecular weights of the reactants. Consider as an example the reaction shown in Equation 6.

$$Pb + PbO_2 + 2H_2SO_4 = 2PbSO_4 + 2H_2O. \qquad (6)$$

This electrochemical reaction produces electricity in the lead-acid automobile battery. Under normal operating conditions, the reaction produces a potential of 2.041 volts. The theoretical energy density as calculated from Equation 5, is 170 watt-hours per kilogram. The practical energy density of this battery system depends on the specific design, but is usually in the range of 15 to 40 watt-hours per kilogram. As a general rule, practical energy densities range from 1/5 to 1/4 of the theoretical values. Table 2 lists the practical energy and power densities for several battery systems. The table also shows that chemical composition affects the cell voltage. Note the increased energy and power densities of the systems containing the lighter elements such as lithium.

Table 2

Battery Characteristics

Battery	Voltage (per cell) (V)	Energy Density (WH/Kg)	Power Density (W/Kg)
Lead-Acid (SLI)	2.04	20-30	50-75
Lead-Acid (Traction)	2.04	10-20	50-75
Nickel-Zinc	1.74	50-70	100
Nickel-Iron	1.37	54	120
Nickel-Cadmium	1.3	15-30	100
Nickel-Hydrogen	1.32	45-50	200-250
Lithium-Titanium Disulfide	2.1	100	TBD
Sodium-Sulfur	2.0	60	30-100
Lithium-Thionyl Chloride	3.6	200-700	400[a]
Lithium-Silver Oxide	2.2	200	1000[a]

Energy density also depends on battery size and rate. Figure 2 is a plot of the energy density as a function of cell capacity at two different rates. Note that the energy density generally increases with increasing battery capacity and, therefore, size and decreases as the rate is increased. The amount of active material relative to the total battery weight increases as a battery is scaled up; less of the total material is needed for the case, terminals, etc. Increased inefficiency at the higher rates is responsible for the decrease in energy density at such rates. In addition, the battery design for a higher rate system differs from that of a low rate system in aspects such as electrode shape and thickness.

Figure 2

Energy density as a function of cell capacity at two different rates.

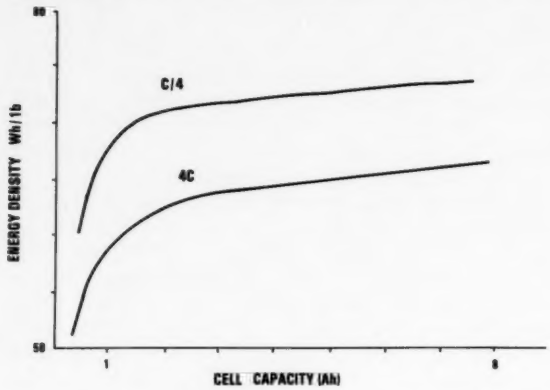

Battery Performance

Ideally, a battery should provide current to the load (external circuit) at a constant voltage until the active components are exhausted. Some batteries do exhibit this type of behavior. Other acceptable systems show different discharge behavior. The shape of the discharge curve depends on the electrochemical reaction and the mechanism by which the reaction occurs. Figure 3 shows the discharge curves for four primary battery systems. Both level and sloping discharge curves can be used; the latter may require an application with a broad voltage tolerance. Certainly, a level discharge behavior gives a higher efficiency. A sloping discharge behavior does make it easier to determine when the end-of-life is near. In fact, one of the interesting issues associated with the lithium-thionyl chloride battery used in heart pacemakers is the need for an end of life indicator. One method is to add another component which discharges at a lower voltage and commences to discharge after the thionyl chloride is exhausted. This combination yields a stepped discharge curve which can be visualized from Figure 3 by looking at the Li/SO_2 followed by the $Li/SOCl_2$ curve.

As would be expected, the exact shape of these curves is dependent on factors other than chemical composition. Figure 4 shows a plot of cell voltage versus capacity for two different current densities. These curves are representative for lithium-thionyl chloride cells. An increase in current density means the electrochemical reaction is proceeding at a faster rate. The higher current gives a larger voltage drop through the total cell resistance leading to a reduced cell voltage. In addition, inefficiencies lead to the lower capacity.

Figure 3

Voltage as a function of capacity (life) over the lifetime of discharge.

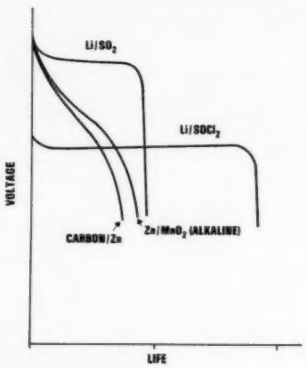

Figure 4

Cell voltage and capacity at two discharge current densities.

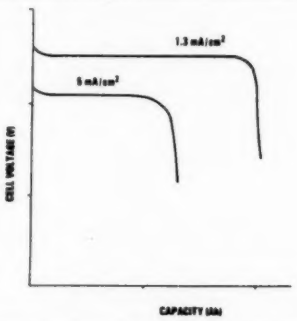

The effect of current (or current density) on capacity is shown in Figure 5. Capacity decreases almost monotonically with increasing discharge current.

Figure 5

Effect of increasing discharge current on cell capacity.

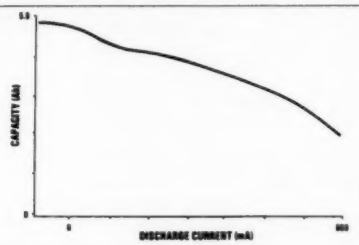

Secondary batteries have both discharge and charge curves. Figure 6 presents typical charge and discharge curves for a nickel-cadmium (NiCd) battery. Note the hysteresis or inefficiency between the charge and discharge processes. The rise in potential at the end of the charge curve is due to the onset of a reaction; in aqueous systems this is often the electrolysis of water. In lead-acid automobile batteries, water electrolysis is a common occurrence. This electrolysis leads to net water loss, hence the need to add water to the non-maintenance free batteries and to the existence under certain conditions of a hydrogen gas danger. The newer maintenance free batteries use electrode compositions and other techniques to reduce water electrolysis. In systems where water electrolysis doesn't occur, reactions at the point of overcharge can lead to degradation of the battery or in the extreme case to battery safety problems.

Figure 6

Typical charge/discharge curves for a secondary battery.

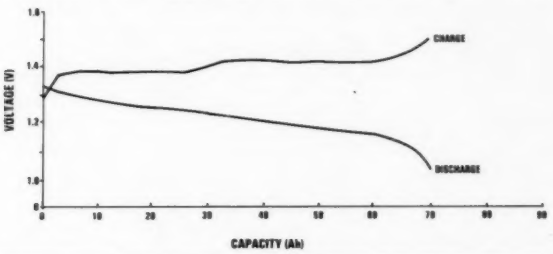

A battery's cycle life is the number of times (cycles) that a secondary battery can be discharged and recharged. Maximum cycle life is necessary to minimize cost, replacement logistics, materials requirements, etc. The cycle life is dependent upon battery design, application, composition, internal battery chemistry, charge/discharge rates and profiles, chemical side reactions, and other inefficiencies. Table 3 gives the cycle life for several secondary battery systems now in use or in development. Entries one and two, the two types of lead-acid batteries illustrate the effect of design and application on the cycle life. The automobile battery (SLI) is required to produce power at relatively high currents for short periods of time in the starting process. This requires a design which enhances current density. The lead-acid traction battery is used in applications such as forklift trucks, golf carts, boats, etc. This battery is designed to provide steady, but somewhat lower currents for longer periods of time and to have a long cycle life.

Zinc-containing batteries all have limited cycle lives because of zinc electrode shape changes which occur on cycling. Satisfactory solutions to this problem have not yet been found. This is one reason the nickel-zinc battery has such a low cycle life.

Table 3

Expected Cycle Life for Some Common Secondary Batteries

Battery	Cycle Life
Lead-Acid (SLI)	200-250
Lead-Acid (Traction)	2000
Nickel-Cadmium	800-2000
Nickel-Zinc	100-150
Nickel-Hydrogen	6000-10,000
Sodium-Sulfur	400-1000
Lithium-Titanium Disulfide	100-200

The last battery listed, lithium-titanium disulfide, is a rechargeable lithium battery system now in the early stage of development. An increase in cycle life can be expected as the system is improved although it may ultimately only reach a few hundred cycles..

Figure 7 shows a relationship which most automobile owners have learned through experience, namely that battery capacity decreases with decreasing temperature. The figure is the relationship for the lead-acid battery. After a battery has been in use for some time the usable capacity drops below the capacity when it was new. This degradation usually happens gradually and results from a number of factors such as loss of active material through flaking, sulfation or irreversible chemical reaction. Then when the temperature drops in the fall or winter, the capacity also drops and one morning the battery has insufficient capacity to start the automobile. In many instances, sufficient capacity can be restored to start the vehicle by warming the battery, either by the use of an external heater or internally through exercise. The battery generates heat during discharge. The application of a small load can, in some cases, warm the battery without removing more power than it makes available.

Figure 7

Temperature effect on capacity.

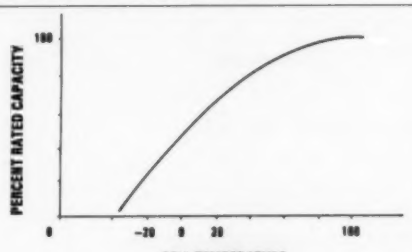

The recharge of a secondary battery involves the forced reversal of the spontaneous electrochemical reaction which produces power. This reaction takes place at the electrode surfaces and leads to a regeneration of the reactants. Because electrodes are designed to optimize the discharge/charge process, the recharging conditions and the best profile for achieving maximum efficiency depend on the battery system. Much effort has gone into the development of optimum charging schemes. These schemes are derived from a knowledge of the effect of factors such as charging rate on the efficiency of the charging process. Figure 8 shows this effect for the lead-acid battery. In a manner somewhat analogous to that of discharge, the extent of charging increases as the charging rate decreases. The gassing voltage is the voltage at which water electrolysis commences and is essentially the charging cut-off voltage. In practice, some electrolysis is advantageous because the gas bubbles produced cause mixing of the electrolyte, reduce concentration gradients, and aid in producing uniform current distribution. Similar information has been collected for other battery systems as well. NiCd batteries tend to exhibit maximum cycle life when subjected to discharge/charge cycles involving relatively high depths of discharge. That is, NiCd batteries are best not left on charge for long periods of time. They should be charged, then used to a relatively high depth of discharge. Lead-acid batteries, on the other hand, float well, that is, can be kept at full charge.

Figure 8

Effect of charging rate on charge accepted for three charging rates.

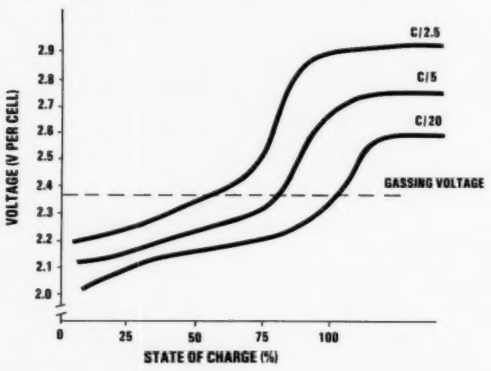

Battery Failure Modes

Batteries fail for a variety of reasons. Table 4 lists a number of such reasons. Electrode consumption and loss of active material may simply be the exhaustion of the chemicals in the battery through normal discharge. For primaries, this means the battery has served its useful purpose. In secondaries and in abnormal behavior of primaries, loss of material can occur from side reactions, flaking, passivation, or other electrical isolation of reactants.

Dendrites are needle-like growths of an electrode material which form under certain conditions during the recharging process when the material is being plated back on the electrode structure. Occasionally these "needles" can penetrate the separator and bridge the gap between the anode and cathode shorting the cell internally.

As mentioned previously, some metals such as zinc undergo a shape change on cycling. Uneven deposition of zinc on the electrode surface and the process of dissolution-reprecipitation results in a net migration of the material. The revised shape of the electrode can cause disruption of the cell structure, strongly nonuniform current densities, and general performance loss.

Table 4

Battery Failure Modes
Loss of Active Material
Erosion
Dendrites
Shape Change
Passivation
Plugging
Electrode Consumption
Shorting
Separator Deterioration

Passivation is the process whereby the active material becomes chemically inert due to the presence of a surface coating or electrical isolation from the internal battery connections. Passivation tends to be a problem in systems containing reactive components such as lithium. Lead-acid batteries passivate through the process of sulfation. Sulfation can occur when lead-acid batteries are operated for prolonged periods in a partial state of charge. In the process, lead sulfate crystals are formed which are larger than the normal high surface area crystals are formed in the discharge process. The large crystals increase cell resistance, cause plate distortion, and do not recharge well.

Some batteries, lithium-thionyl chloride, for example, produce a solid product at one of the electrodes on discharge. This product can plug the porous structure of the electrode reducing the electrode surface area and, ultimately, stopping the reaction.

Separator deterioration or penetration or other internal structural failures, whether chemically produced or from abuse, can cause anode-cathode contact producing

short circuits in the same way as dendrite penetration. Obviously, battery engineers design the systems to minimize the chances of premature battery failure.

Testing

Most battery systems undergo extensive testing, not only in the initial phase of their development and production, but throughout the lifetime of their production and use. The specific nature of the testing depends to a large extent on the application. These tests are performed by the manufacturer and the customer. Tests commonly include the measurement of the quantities which have been discussed in this article including voltage, current, capacity, efficiency, temperature effects and cycling.

A major emphasis of any test program is the determination of the safety of the system and the scoping of the limits of abuse which the battery can safely accommodate. This aspect is increasing in importance because of the increasing use of high energy electrochemical reactions based on reactive materials such as lithium.

Terminology

A short glossary follows of the terms most often encountered when considering batteries. More extensive lists exist elsewhere (see the first two listings in the Bibliography, for example) for anyone interested in pursuing the subject further.

Active material: the constituents which contribute to the electrochemical reaction and hence the battery's power output; these include the anode, cathode and in many cases, the electrolyte.

Anode: the electrode at which oxidation (loss of electrons) occurs; the anode is the negative terminal during discharge.

Capacity: the ampere-hours that can be withdrawn from a battery; rated capacity is defined by the manufacturer at some temperature, discharge rate and cut-off voltage; available capacity is the capacity that can be used at a given set of conditions.

Cathode: the electrode at which reduction (gain in electrons) occurs; the cathode is the positive terminal during discharge.

Charge/Discharge Rate: the current applied/removed to charge/discharge a battery, usually normalized to the rated capacity; rates are usually written as the capacity C divided by the time in hours, e.g. C/4, 2C, etc., where C/4 is the 4 hour rate, 2C is the one-half hour or 30 minute rate.... The current is found by dividing the capacity by the rate; for example, a 500 ampere-hour (Ah) battery charged or discharged at the 10 hour rate (C/10) would involve a current of 500/10 or 50 amperes. Two cautions are in order here. First, the time required to charge fully a battery will likely exceed that given in the rate. That is, a battery being charged at the 10 hour rate, C/10, will require more than 10 hours to reach full charge. This is the result of inefficiencies. Second, care must be taken when calculating the current from the rated capacity and time because the rated capacity is determined at a given set of conditions. For example, a battery with a rated capacity of 100 Ah at the C/5 rate may only give 90 Ah at the higher C/3 rate. The C/3 rate would actually be 30A not 33.3A.

Current Density: the current per unit area of electrode; current density is usually quoted as amperes (or some unit thereof) per square centimeter of electrode, e.g., 60 mA/cm^2.

Cut-off Voltage: the voltage at which a discharge or charge is terminated; manufacturers may specify a cut-off voltage to prevent battery damage or an unsafe condition.

Depth of Discharge: the ampere-hours removed as a percentage of rated capacity; when 80 Ah are removed from a 100 Ah battery, the depth of discharge is 80%.

Efficiency: the ratio of ampere-hours or energy removed to the respective amounts required to restore the initial capacity; for voltage it is the ratio of the average discharge voltage to the average charging voltage.

Electrolyte: the ionically conducting medium in contact with the two electrodes which serves to provide the electrical circuit connection within the battery; it may be solid or liquid; usually a salt is dissolved in a solvent to produce it.

Energy Density: the ratio of the rated energy normalized to weight or volume; it is a measure of how much energy can be removed from a battery; the term specific energy is also used interchangeably.

Polarization: the deviation between the operating voltage and the open circuit voltage of a battery.

Power Density: the ratio of rated power to weight or volume; it is a measure of how fast energy can be removed from the battery; specific power is another term sometimes used.

Bibliography

1. *Handbook for Battery Energy Storage in Photovoltaic Power Systems*, prepared by Bechtel National, Inc., available from NTIS as SAN-2192-TI or SAND80-722, February 1980.

2. Scott, W. R. and Rusta, D. W., "Sealed-Cell Nickel-Cadmium Battery Applications Manual," *NASA Reference Publication 1052*, December 1979.

3. Modern Electrochemistry, J. O. M. Bockris and A. K. N. Reddy, Plenum Press, N.Y., Vol. 2, pp. 1401-1432, 1970.

4. Kalhammer, F. R., Energy Storage Systems, *Scientific American, 241* (1979), p. 56.

5. Birk, J. R., Klunder, K. and Smith, J. C., "Superbatteries: a Progress Report, *IEEE Spectrum, 16* (1979), p. 49.

Profiles in Science

Dr. Mark S. Wrighton is the Frederick G. Keyes Professor of Chemistry at the Massachusetts Institute of Technology. He is renowned for his pioneering research toward the conversion of solar energy into chemical fuels and electricity. Professor Wrighton's many publications are in the fields of inorganic photochemistry, catalysis, photoelectrochemistry, and surface chemistry. Currently, he is a principal investigator for the Office of Naval Research working in two areas: (a) photochemical activation of catalysts and surface photochemistry and (b) electrochemical studies of chemically functionalized microelectrodes and the behavior of microelectrodes. This research has significantly contributed to the understanding of photochemical and photoelectrochemical processes and has provided the basis for the development of improved catalysts and electrodes for the control of chemical synthesis of naval materials.

Professor Wrighton, who started teaching at M.I.T. in 1972 after receiving his doctorate from the California Institute of Technology, is the youngest person to ever hold a named chair at M.I.T. Included among his many honors and awards are: E. O. Lawrence Memorial Award, Department of Energy; New York Academy of Sciences Halpern Award in Photochemistry; in 1983 he was selected to be a MacArthur Prize Fellow.

Spectroscopic Studies of Electrochemical Interfaces

By E. Yeager, B. D. Cahan, D. Scherson and M. Hanson
Case Center for Electrochemical Sciences, Case Western Reserve University

Introduction

Research in electrochemistry is undergoing a renaissance. In part, this renaissance is stimulated by the recognition of the technological importance of electrochemistry in such areas as the electrowinning of aluminum, batteries, corrosion control, electrochemical machining, and electrochemical sensors. Equally important to the renaissance are indications that research on electrochemical interfaces has reached a critical stage where especially rapid development of this surface science is likely to follow over the coming ten years. This optimism reflects the impact that both *in situ* and *ex situ* surface chemical physics techniques are starting to have on the studies of electrochemical interfaces.

In many electrochemical reactions, the electrode surface not only serves as a source or sink for electronic charge but also provides sites for the adsorption of reactants, intermediates, and products. Thus, the electrode surface plays a catalytic role. Illustrations of such electrocatalytic reactions include the electro-generation of H_2 and O_2 in water electrolyzers, the reduction of O_2 in fuel cells and batteries, the electro-generation of chlorine gas, and various electro-organic oxidation and reduction reactions. Relatively little information is available, however concerning the specific adsorption sites and the interactions of adsorbed species with these sites.

Electrochemical methods involving current—charge—potential measurements provide a sensitive tool for detecting the electrochemical adsorption of various species on electrode surfaces but lack molecular specificity. To illustrate, consider the adsorption of hydrogen on polycrystalline platinum, one of the most extensively used electrocatalysts.[1] The voltammetry curve in Figure 1 represents the current while linearly sweeping the applied potential cyclically in the positive and negative directions. Hydrogen atoms appear to be electrosorbed according to the reaction:

$$2H^+ + 2e^- \rightleftharpoons H(ads) \qquad (1)$$

during the potential sweep from 0.4 to 0.0 V while the reverse process appears to occur during the sweep over this range in the opposite direction. Up to five hydrogen desorption peaks have been deconvoluted from the desorption curve. The question is then what causes these multiple peaks. Are they due to adsorption on different crystal planes, different sites on a given crystal plane, induced heterogeneity, competitive adsorption of other species such as anions, etc.? As discussed later in this article, these questions are still answered ambiguously.

The structure in the voltammetry curve in Figure 1 as the potential is swept to more positive values (> 0.8V) is attributed to the formation of an anodic film involving adsorbed oxygen species such as O and OH from water. During the subsequent reverse sweep, this film is very irreversibly reduced. The structural features of this film are also not well understood, despite its importance to the electrocatalytic properties of platinum.

Figure 1

Voltammetry curve for polycrystalline platinum in a thin-layer electrochemical cell with an αPd/H counter-reference electrode. Potentials are expressed relative to the reversible hydrogen electrode. Electrolyte: 0.05 *M* H_2SO_4; electrolyte gap: 10^{-3}cm; temperature: ~25°C; voltage sweep rate: 20 mV/s (W. O'Grady et al.[2]).

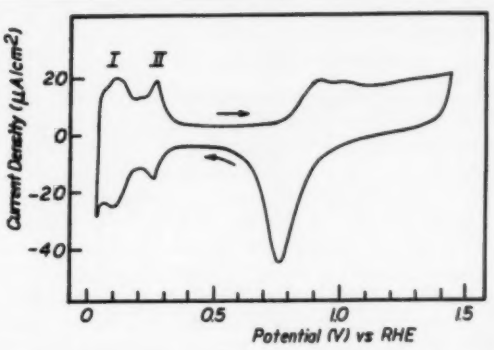

ONR (Office of Naval Research) has played a key role in supporting research leading to the development of various spectroscopic techniques for electrochemical studies and their use. The research in the authors' laboratories in this area has been supported by ONR. This article will discuss some of the promising *in situ* and also *ex situ* spectroscopic techniques that have been involved in this research.

In situ Spectroscopic Techniques

Ultraviolet-Visible Reflectance Spectroscopy

Ultraviolet-visible reflectance spectroscopy lends itself to *in situ* studies of electrode surfaces since most electrolytic solutions are transparent to such radiation. Both external and internal reflectance techniques have been used (see Figure 2). The former has found more frequent use but the latter permits the excitation of surface plasmons. The shifts in the surface plasmon resonance are measured from the dependence of the reflectance on the angle of incidence. The surface plasmon resonance frequencies are sensitive to changes in the electrode surface and adsorbed species.[5]

A frequently used cell arrangement for external reflectance spectroelectrochemical measurements in the authors' laboratories is shown in Figure 3. The cylindrical cell facilitates measurements at various angles. The changes in reflectance produced by changes in the electrode potential are measured as a function of wavelength. The relative reflectance changes ($\Delta R/R$) are small (e.g. 10^{-4}/V) but still quite easily measured with modern electronic techniques. These optical changes arise from several effects:

— an intrinsic electroreflectance effect associated with the change in the surface charge density on the electrode;

— the optical properties of species which form adsorbed layers on the electrode surface;

— changes in the structure of the double layer and particularly the state of the solvent in the compact double layer;

— the formation of passivation layers on metals

— surface roughening.

With most adsorbed species at mono- and submono-layer levels, most of the change in reflectance with potential is caused by the change in surface charge. The truncation of the conduction band orbitals at the metal electrode surface results in an evanescent wave extending into the interface as shown in Figure 4. When the charge in the metal is changed, the extent to which the evanescent wave extends out from the metal surface changes. Curve A in Figure 4 indicates the electron density extending into the interface when the potential corresponds to zero charge (PZC). When the potential is negative to this value, the electron density extends further into the interface as shown by curve B while at potentials positive to this value the electron density is represented by curve C. This transition region at the interface acts like an optical layer of thickness, small compared to the wavelength with its optical properties dependent on potential. The adsorption of species on the electrode changes the surface charge, and modifies the optical properties of this transition region. In fact, this effect rather than the intrinsic optical properties of the adsorbed species is usually the principal source of the reflectance changes produced by adsorbed species.

Figure 2

Configuration for external reflectance (A) and internal reflectance (B,C) spectroscopic studies of electrode surfaces. Configuration C (Otto[3]) requires a transparent prism to be positioned within a small fraction of a wavelength from the electrode surface while configuration B (Kretschmann[4]) requires taht the metal film electrode in the prism be sufficiently thin to be transparent to the radiation.

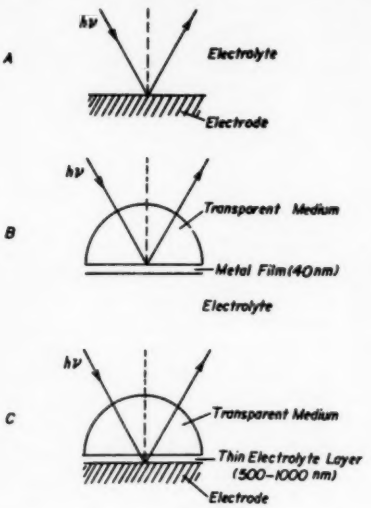

Figure 3

Top view of configuration of cylindrical cell for optical and electrochemical studies used at CWRU.

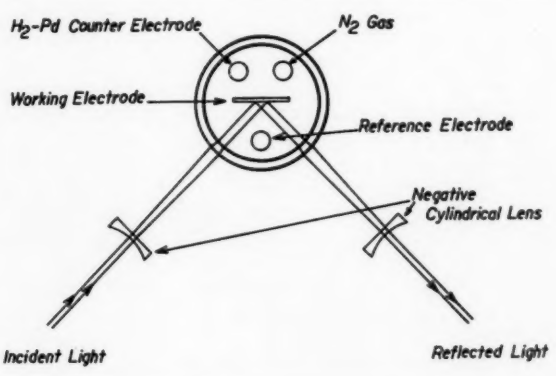

Figure 4

Electron density versus distance at a metal electrode surface. Curve A: at potential of zero charge (pzc). Curve B: at potential negative to pzc. Curve C: at potential positive to pzc.

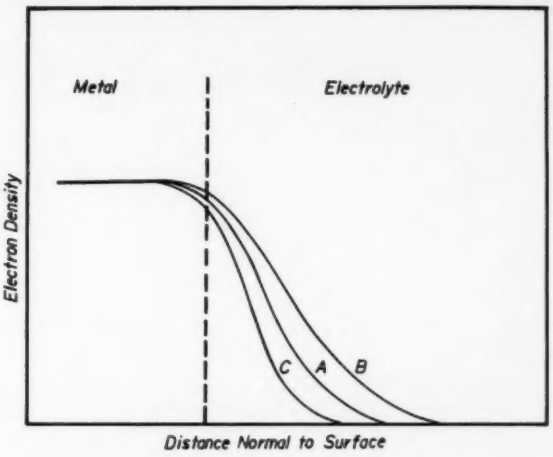

Figure 5

Reflectance spectra of Fe(III)-TsPc in 0.1 *M* NaOH adsorbed on the basal plane of stress-annealed pyrolytic graphite electrode at 0.90 V (A) and at Pt electrode at 0.70 V (B) with Ar-(————) and O_2' (—) saturated solutions (B) (Nikolic *et. al.*[6]).

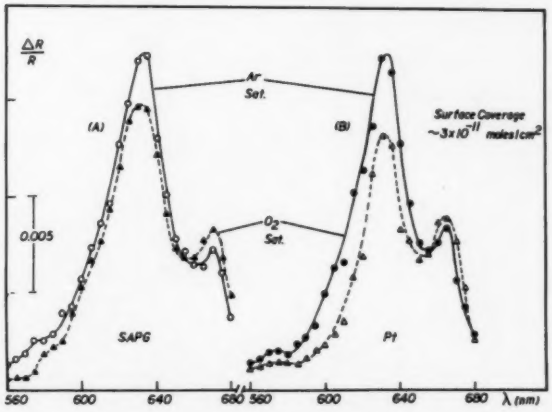

With adsorbed species with high molecular extinction coefficients ($\epsilon > 10^4$), however, the spectra of even just a monolayer can be observed directly by reflectance techniques. For example, Figure 5 indicates the absorption spectra of a water soluble transition metal macrocycle (iron tetrasulfonated phthalocyanine, Figure 6) adsorbed at monolayer levels on polycrystalline platinum and on the basal plane of highly ordered graphite. This species is so strongly adsorbed that the pre-adsorbed layer is retained on the surface even though the solution in contact with the electrode is free of this macrocycle. This macrocycle adsorbed on graphite is a very effective catalyst for the four-electron O_2 reduction. The spectra in Figure 5 provide evidence that the complex is adsorbed with the plane of the ligand perpendicular to the surface as is discussed later in this article.

Figure 6

Iron tetrasulfonated phthalocyanine (FeTSPc).

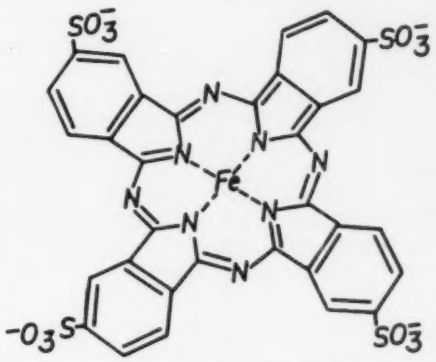

Another interesting system studied with UV-visible reflectance techniques at Case Western Reserve University (CWRU) is the underpotential deposition of metals at mono- and submonolayer levels on foreign metal substrates. These layers are often formed at potentials quite positive to those necessary for the deposition of the bulk metal because of the strong interaction of the metal atoms with the substrate metal. Figure 7 indicates the spectra for the adsorbed lead atoms on gold at various solution concentrations of lead. The surface coverage with lead depends on the solution concentration of lead. An isosbestic point is evident at a wavelength of ~500 nm, where the reflectance is the same for the gold surface with and without adsorbed lead atoms. The optical properties of the lead covered gold-electrolyte interface do not correspond to either lead or gold and are quite unique. Such underpotential deposited layers have unusual catalytic properties for such processes as O_2 reduction and electro-organic oxidations.

Optical reflectance measurements can also be used to examine the kinetics of the adsorption and desorption of various species. If the electrode potential is a.c. modulated, the reflectance is also modulated with a frequency dependence which can be used to examine the ad-

sorption-desorption kinetics. The adsorption-desorption kinetics can be represented by an equivalent circuit as shown in Figure 8, where C_{ad} is a capacitive component which depends on the adsorption isotherm, r_{ad} is a resistive component representing the kinetic control and W is the Warburg impedance (which is equivalent to a transmission line) representing the diffusion of the adsorbate to and from the electrode surface. The double layer capacitance associated with the interface is represented by C_d while r_e is the bulk solution phase resistance. The a.c. modulation of the intensity of the reflected light provides a direct measure, of the modulation of the surface concentration of the adsorbed species and hence, the charge in C_{ad}. A knowledge of C_d in the presence of the adsorbed species is not required, thus avoiding a major problem in such kinetic studies just using electrochemical methods. This technique lends itself to Cole-Cole type plots of the imaginary vs. real components of the electroreflectance $\rho = (1/R)(dR/dE) = \rho_1 + i\rho_2$. With pure kinetic control without diffusion control, a semicircle is obtained (Figure 9A) while with diffusion control a quarter circle is obtained (Figure 9B). The high frequency limit of the real component corresponds to the intrinsic electroreflectance coefficient, *i.e.*, the change of the relative reflectance at constant coverage with the adsorbed species $[\rho_1 = (1/R)(\partial R/\partial E)_\theta]$. Combined kinetic and diffusion control results in complex plane plots of the type shown in Figure 9C for the adsorption of underpotential deposited lead on gold.

Figure 7

Wavelength dependence of normalized reflectance change for the UPD of lead on polished gold for various $Pb(NO_3)_2$ concentrations in 0.2 ***M*** $HClO_4$ at 0.33 V vs. NHE. Data evaluated from reflectance vs. potential curves obtained with sweep rate of 20 mV/s (Adzic ***et al.***[7]).

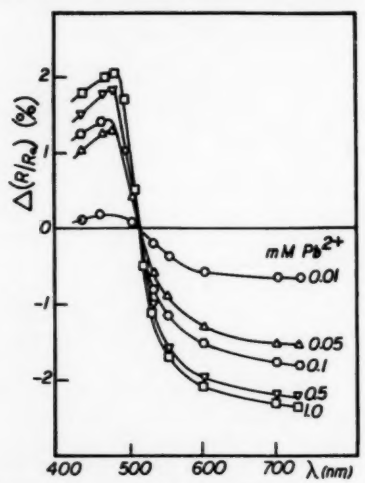

Figure 8

Equivalent circuit for adsorption-desorption kinetics C_d – double layer capacitance; C_{ad} – adsorption capacitance; r_{ad} – resistance representing adsorption – desorption rate process; W – Warburg impedance representing diffusion of adsorbate to and from electrode surface; r_e – bulk solution phase resistance.

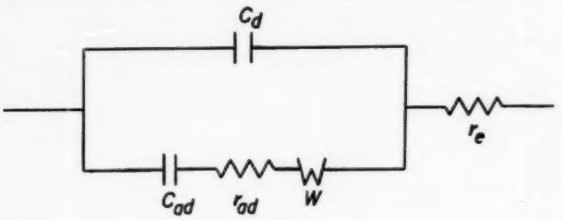

Figure 9

Complex plane plots of electroreflectance admittance:
A. Theoretical curve for pure kinetic control
B. Theoretical curve for pure diffusion control
C. Experimental plot for underpotential deposition of lead on evaporated gold electrode in 1 ***mM*** $Pb(NO_3)_2$ + 1M $HClO_4$ at λ = 600 nm and a time average potential of 0.268V vs. NHE at 25°C (Adzic ***et al.***[8]).

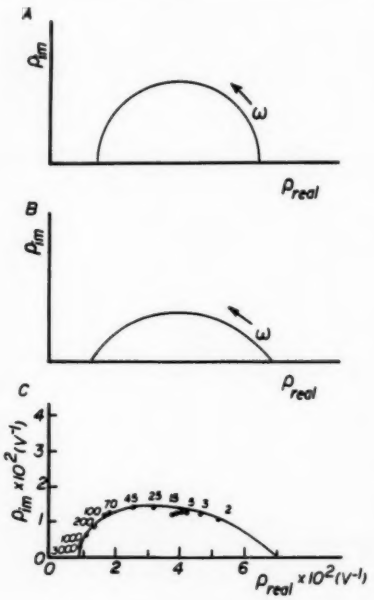

Ellipsometric Spectroscopy

A particularly attractive optical reflectance technique is ellipsometry. Elliptically polarized light is reflected from the electrode surface and the change in azimuth and eccentricity measured. An automatic ellipsometer has been developed by Cahan and Spanier[9] which uses a high speed rotating analyzer and affords a high data collection rate (one data point per 20 millisec). With this instrumentation and a stepping monochromator, the automatic ellipsometer can be used for spectroscopic measurements. This ellipsometer measures the reflectance change as well as the ellipsometric parameters. When the surface under study can be satisfactorily approximated as two semi-infinite media separated by an optically homogeneous thin film, these data are sufficient to calculate the real and imaginary components of the optical dielectric constants and the thickness without any other assumptions or data[10].

The automatic ellipsometer is a particularly powerful tool for *in situ* studies of the passivation film on metals such as iron. Figure 10 indicates the wavelength dependence of the dielectric constant for the 3-nm thick passivation film formed on iron in a borate buffer solution. These data together with considerations involving the Kramers-Kronig relation provide evidence for a strong adsorption band above 5 eV. The 3d orbitals are relatively narrow and probably fall in a relatively wide gap.

The Cahan-Spanier automatic ellipsometer has sufficient sensitivity to detect a very small fraction of a monolayer (e.g., less then 10^{-2} of a monolayer). The model of an optically homogeneous layer separating two semi-infinite phases, however, is no longer valid. A need exists for models for mono- and submonolayers relating the ellipsometric measurements to the electronic properties of such adsorbed species and the metal and electrolyte phases.

Vibrational Spectroscopy

An important development in electrochemistry over the past decade has been *in situ* Raman and infrared reflectance techniques for obtaining the vibrational spectra for adsorbed species and layers at electrodes. The initial research on the Raman technique and the critical work on the infrared have been carried out at the University of Southampton (England) by M. Fleischmann and A. Bewick, with the support of ONR.

In situ infrared studies using internal attenuated total reflectance were already carried out with semiconductor transparent electrodes in the 1969's in the authors' laboratory[11, 12]. The C-H stretch peaks were detected for adsorbed layers of higher molecular weight molecules such as octanol, stearic acid, and surfactants on germanium electrodes using D_2O as the solvent to minimize solvent interference. With semiconductor electrodes of sufficient transparency in the infrared, however, most of the potential drop was in the space charge region in the electrode phase and relatively little information was gained concerning the adsorbed species. Furthermore, solvent absorption in the infrared imposed severe restrictions. These measurements, however, did yield data concerning the optical properties of the space charge region in the semiconductors.[12].

Figure 10

Complex dielectric constant ($\epsilon_1 - i_2$) of passive film on iron grown in borate buffer at pH 8.4 at 1.15 V and measured at 1.05 V vs. RHE (1 atm). Determined with automatic ellipsometer. Angle of incidence: 70° [Cahan and Chen[31]].

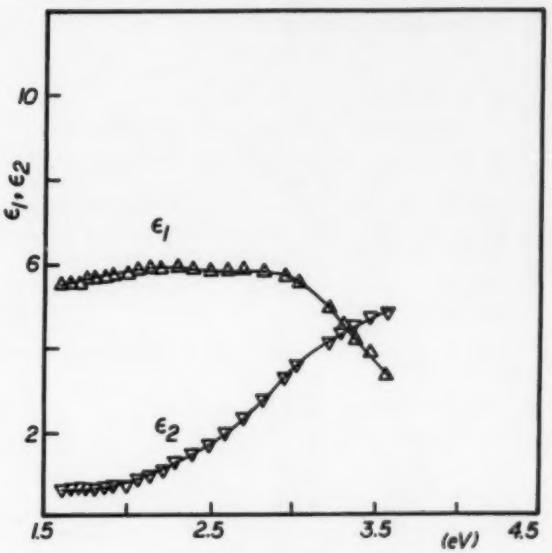

More recently Bewick et al.[13, 14] have used external infrared reflectance spectroscopy with a very thin electrolyte layer combined with square wave modulation of the electrode potential to study the water layer adjacent to the interface and hydrogen adsorption on Pt in acid media. A typical spectroelectrochemical cell[15] for each infrared studies is shown in Figure 11. For the more weakly bound H (voltammetry peak I in Figure 1) the vibrational data provide evidence of a strong interaction between the adsorbed H and water of the form Pt-H-OH_2. The strongly bound H (Peak II in Figure 1) shows metallic like behavior on the basis on the sign and magnitude of the reflectance change with coverage. Beweick et al.[16] suggest a screened proton model with the electron of the hydrogen atom delocalized in the conduction band of the metal. The adsorption of other species including CO on platinum electrodes has also been examined with electromodulation techniques.[14]

Three types of *in situ* infrared reflectance techniques have been used by the Southampton electrochemists to examine adsorbed species on electrode surfaces.

EMIRS: (electrochemically modulated infrared reflectance spectroscopy) Square wave modulation of the potential leads to a differential spectrum as a result of the adsorption—desorption of the species under study and the modulation of the amplitude and frequency of the infrared absorption peaks.

IRRAS: (infrared reflectance absorption spectroscropy) The infrared radiation is modulated between parallel (P) and perpendicular (S) polarizations relative to the plane of reflectance with high angles of incidence. The P polarized radiation is sensitive to species at distances from the interface, small compared to the wavelength while the S polarized radiation is not. Thus, the difference signal is selectively sensitive to adsorbed species.

SNIFTIRS: (subtractively normalized interfacial Fourier transform infrared spectroscopy) The difference spectra between two potentials is recorded with P-polarized light with 4 to 8 interferometric scans at each potential and the difference signal obtained with digital subtraction. The sequence is then repeated until an adequate signal-to-noise ratio is achieved.

Figure 11

Infrared cell for ***in situ*** electrochemical studies (Pons[15]).

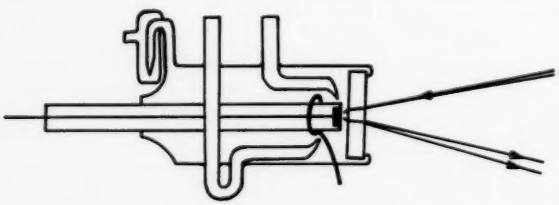

The types of spectra obtained with the EMIRS and IRRAS techniques are illustrated for CO adsorbed on platinum in Figure 12. Note that for adsorbed species, only dipole oscillators with a non-zero component perpendicular to the surface are active.

Multiple internal reflectance infrared with Fourier transform has been used by Neugebauer et al.[17] to examine *in situ* the oxidation of iron electrodes in alkaline electrolytes.

Since the observation of unusually strong Raman signals for pyridine adsorbed on silver electrodes by Fleischmann et al.[18, 19] and Van Duyne et al.[20] in the mid 1970's, great interest has developed in Raman studies of adsorbed species on electrode surfaces. Many publications[21] have appeared, mostly concerned with experimental and theoretical studies of possible mechanisms for the extraordinarily large surface enhanced Raman scattering (SERS) observed with many adsorbed molecules on Ag and, to a lesser extent, Cu, Au and Li. The enhancement effects are observed at metal-vacuum as well as metal electrolytic interfaces which have been roughened.

A number of explanations have been offered for SERS[21]. More than one mechanism is likely involved. The first class of proposed enhancements mechanisms is based on geometrically defined surface optical resonances which involve free electron like metals with rough surfaces. Large enhancement of the optical electron fields is realized at the roughened surface of such metals if the incident radiation is in resonance with normal modes of the conduction electrons. The adsorbed molecules are subjected to these greatly enhanced optical frequency fields and are expected to exhibit much enhanced Raman signals on roughened surfaces relative to smooth surfaces. The second class of enhancement mechanisms involves new and modified electronic states resulting from the interaction of the adsorbed species with the substrate metal. These interactions provide new excited electronic energy levels and can lead to resonance Raman effects involving electron transfer between the metal and adsorbate. With adsorbates such as pyridine exhibiting 10^5 to 10^6 fold enhancement on silver, both types of enhancement mechanisms appear to be involved. Using single crystal silver surfaces, Campion et al.[22] in ONR sponsored research has found no enhancement with smooth surfaces for physical adsorbed pyridine at low temperatures beyond that expected for a near ideal optical reflector using the Drude-Fresnel equations.

With the discovery of SERS in the 1970's, Raman spectroscopy was expected to have a major impact on surface studies and particularly electrochemical adsorptive studies. The uncertainty concerning the mechanisms for SERS, however, has seriously limited its usefulness. There is often no assurance that the observed Raman spectrum for an adsorbed species on a given surface corresponds to a majority species or adsorption on the predminant sites. The enhancement can be by a factor of 10^6, and a minority species or a minority site may be predominant in the observed spectrum. Furthermore, Raman techniques are generally limited to the study of most adsorbed species on only a few metals (Ag, Cu, Au). Adsorbed species involving an intrinsic resonant Raman effect can exhibit sufficiently strong Raman signals to facilitate their study on surfaces not exhibiting significant SERS and not roughened. The interaction of these species with the surfaces, however, perturbs the electronic states involved in their intrinsic resonant Raman. This results in changes in the enhancement with the type of adsorption site and seriously complicates quantitative studies.

Figure 12

Infrared spectrum of CO adsorbed on platinum in 1 *M* $HClO_4$ (Bewick[14]).
a. Infrared reflectance absorption (IRRAS) spectra at 650, 450, 250 and 150 mV (left to right) vs. NHE.
b. IRRAS difference spectrum: + 50 mV from + 450 mV.
c. Electrochemically modulated infrared spectroscopy (EMIRS) for modulations + 50 mV to + 450 mV.

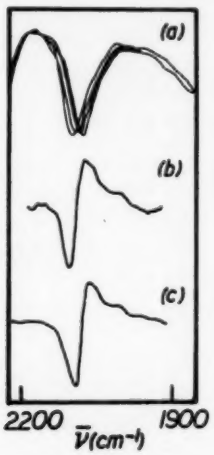

Even with these restrictions, Raman spectroscopy has proved a useful *in situ* tool for the study of adsorbed species on electrode surfaces in various laboratories including the authors. Raman spectroscopy has been particularly effective in the study of the macrocycles adsorbed on electrode surfaces[23]. These complexes are of interest as catalysts for O_2 electroreduction. The Raman spectra have been examined on the low index surfaces of single crystal silver (see Figure 13). The intensities are dependent on the crystal plane, the polarization of the laser beam and the electrode potential. The Raman spectra of the adsorbed species are similar to these for the solution phase in regard to the principal peak frequencies but differ in the relative intensities of the peaks. The *in situ* Raman data provide evidence that the cobalt and iron complexes are adsorbed on the surface with the plane of the macrocycle ligand normal to the electrode surface.

Extensive studies have also been carried out in the authors' laboratory on the adsorption of para-nitroso dimethyl aniline on metal electrodes in electrolytes and also at the solid-gas interface for insulators and semiconductors.[24] Such adsorbed species can be used as probes of the Lewis acid-base properties of the surfaces by examining the extent to which the Raman spectra indicate quinoid vs. aromatic character (see Figure 14). The Bronsted acid-base properties have been probed with para-dimethyl aminoazobenzene.[24]

The formation of oxide films on silver electrodes have been examined *in situ* at CWRU using Raman spectroscopy.[25] These studies indicate that the divalent Ag_2O_2 can be generated photochemically by the laser beam (λ = 488.0 nm) from the monovalent Ag_2O on a silver electrode in an alkaline electrolyte.

The vibrational frequencies of a number of species (e.g., pyridine, pyrazine, para-nitroso dimethyl aniline, cyanide) adsorbed on electrode surfaces have been found to shift in a linear manner with changes in the electrode potential.[26] Several models have been proposed for these frequency shifts. Molecular orbital calculations using the atom superposition—electron delocalization (ASED) method have been carried out at CWRU for CN^- adsorbed in silver.[27] The model has involved Ag clusters (Ag_4 and Ag_7) with the CN^- interacting with various sites. In this calculation, the C and N ionization potentials are fixed, and the Ag ionization potentials are shifted in response to the applied electrode potential. The frequency shifts with electrode potential for the C-N^- and Ag-C harmonic band stretching force constants are caused by changes in the contribution of the C-N^- antibonding orbital ρ_p^* as a function of a potential. This is the equivalent of a Stark effect.

Figure 13

Raman spectral components obtained from the adsorbed Fe-TSPc on: Ag(100), Ag(111), and Ag(110).
Potential: 0.2V vs. SCE, 25°C.
Electrolyte: 0.1 *M* $HClO_4$ (Ar saturated).

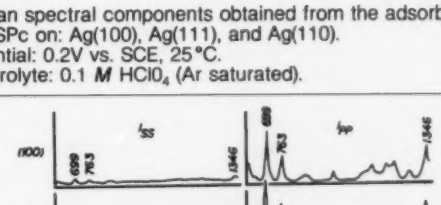

Figure 14

Probe molecules exhibiting resonance Raman.

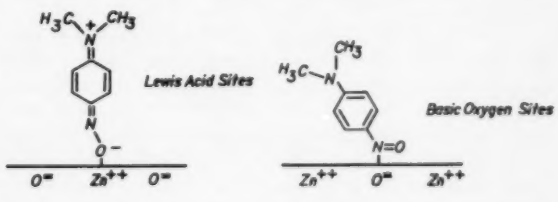

Photoelectrochemical Processes

Most of the interest in photoelectricity has been the result of the possible use of such processes for energy conversion. The wavelength and potential dependence of such processes, however, yield interesting information concerning band bending, surface states, and other electronic features of semiconductor electrodes of importance to the understanding of the overall electrochemistry of such interfaces. Photoemission from metals into electrolytes also has been studied by electrochemists but so far has yielded relatively little information concerning adsorption and electrocatalysis. These aspects of photoelectrochemistry deserve more attention.

Mossbauer Effect Spectroscopy

Mossbauer effect spectroscopy, which involves the resonant absorption or emission of nuclear gamma radiation, has been applied to *in situ* studies of adsorbed species and layers containing elements to serve as either Mossbauer emitters or absorbers, e.g. Fe, Co. The Mossbauer spectra provide insight into spin states and coordination to these elements. Particularly interesting *in situ* results have been obtained for the passivation layers on iron in electrolytic solutions by Dr. W. O'Grady[28] of Brookhaven National Laboratory and more recently by Professor R. Hoffmann and his research group[29] at CWRU, the latter in conjunction with a grant from the ONR Selected Research Opportunities Program. Both groups have used transmission techniques with very thin films of iron supported on gold-coated polymer films as the passivated electrodes in a borate buffer electrolyte. The CWRU group have also developed an emersion technique[30] in which a vertically mounted iron disk electrode is rotated about an horizontal axis with the lower part of the disk submerged in the electrolytic solution (see Figure 15). The Mossbauer spectrum is then observed for a section of the disk above the electrolyte using the electron yield as a measure of the Mossbauer absorption. The thin film of electrolytic solution covering the electrode surface as well as the vapor of the solution attenuate the electron current, but the observed electron current is still a measure of the γ-ray absorption. This technique has the advantage that it can be used with bulk iron and ferrous alloy electrodes and is selectively sensitive to the region near the electrode surface since the electrons have quite limited escape depth from the metal. While not strictly an *in situ* method, this emersion technique has some of the features of such.

The Mossbauer data provide strong evidence that the passivation film formed on iron in aqueous electrolytes has an amorphous polymeric-like structure and not the well developed crystal structure found in *ex situ* electron microscopy diffraction studies. The passivation films on iron appear to develop crystal structures in the vacuum environment of the microscope. This has been verified at CWRU using a high voltage transmission microscope equipped with an environmental cell which permits the examination of the passive layer on iron in a humidified air or humidified rare gas environment.[32] The electron diffraction pattern shifts from diffuse rings to a spot pattern characteristic of well developed crystals when the sample is subjected to the vacuum in the presence of the electron beam. This points out the need for *in situ* techniques.

The CWRU group have also developed an *in situ* Mossbauer cell arrangement for electrochemical studies of iron and cobalt containing electrocatalysts in high area carbon or graphite porous electrodes of the types used in fuel cells and batteries.[33] With this system, it has been able to record the changes in the iron macrocycle electrocatalysts as functions of electrolyte, potential and time. These measurements have been used also to examine the degradation of these catalysts and the effect of heat treatment of the catalysts.

Figure 15

Apparatus for Mossbauer measurements using conversion electron and the emersion electrochemical techniques.

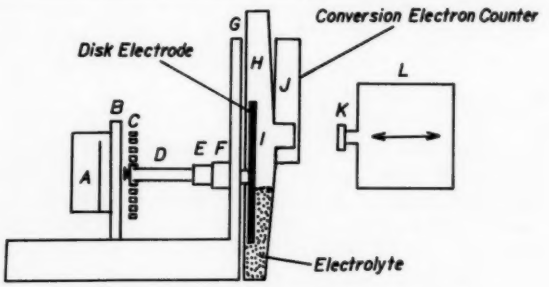

Extended X-ray Absorption Fine Structure (EXAFS)

EXAFS involves the measurement of the fine structure in the X-ray absorption spectra just above the absorption edge and arises from the interference effects associated with scattering of the X-ray photoelectrons from surrounding atoms. By relatively straightforward computational transform techniques, the radial distribution functions can be obtained for the nuclei surrounding the species responsible for the absorption. This technique can be used for the *in situ* examination of adsorbed species and various layers on electrodes by measuring either directly the absorption of the X-rays or measuring the X-ray fluorescence as an indication of the absorption. The element involved in the absorption, however, usually must be present in substantial quantities only in the adsorbed layer. Otherwise the deconvolution of the data into two sets of radial distribution functions is necessary and this can present severe signal-to-noise requirements. With *in situ* studies of the passivation film on iron, Professor Hoffman and his students have used a thin film of

iron less than 10-nm thick electrodeposited on a thin capor deposited gold layer on a Mylar film and then measured the fluorescence. This research group has also carried out quite successfully EXAFS measurements using an emersion technique with a vertical rotating disk similar to that developed by this group for Mossbauer studies. The X-ray absorption is measured in terms of electron yield current and is sensitive only to the surface layers. The results[34] obtained with this technique by Professors Hoffmann and J. Mann (also of CWRU), using the Stanford synchrotron, provide evidence that the passive film on iron lacks long range order and is not a crystalline oxide; this supports the Mossbauer results. EXAFS also appears promising as a technique for examining electrocatalysts such as the transition metal macrocycles adsorbed on high area carbon electrodes.

Electrochemical Studies with *ex situ* Surface Physics Techniques.

The electrochemical properties of solid metal and semiconductor electrodes are strongly dependent on the crystal planes. To achieve a full understanding of electrocatalysis, it is essential to carry out electrochemical studies on single crystal surfaces free of impurities and also with intentionally adsorbed impurities. *In situ* techniques for examining the surface structures for single crystal electrodes are generally lacking in the electrochemical environment. The electrochemist needs techniques such as low energy electron diffraction (LEED) for single crystal electrode studies to establish what restructuring may occur and to examine ordering phenomena in adsorbed layers. LEED, however, is limited to the vacuum environment. Other surface physics techniques such as Auger electron spectroscopy (AES) and X-ray and ultra violet photoelectron spectroscopies (XPS and UPS) are needed to provide information concerning elemental analysis and the chemical environment at the electrode surface with polycrystalline and amorphous electrodes as well as single crystal electrodes. These techniques, however, are also restricted to the vacuum environment. Furthermore, the procedures for preparing various low and high index single crystal surfaces are well worked out in ultrahigh vacuum for many solids. This is not the situation in general for the electrochemical environment.

These factors have prompted several electrochemical research groups to prepare and characterize single crystal electrode surfaces free of impurities *in vacuo* using LEED, AES and in some instances XPS. Then these surfaces are transferred into the electrochemical environment using techniques designed to minimize the possibility of restructuring and contamination of the surfaces during the transfer. Following electrochemical characterization, the electrode surfaces are then returned to the ultrahigh vacuum environment for re-examination with various surface physics techniques. The electrochemical measurements are carried out with a minimum amount of electrolyte solution either in the same vacuum chamber or an adjacent chamber (filled with an inert gas) without the electrode being exposed to air either before or after the electrochemical measurements. Following the electrochemical measurement, the single crystal electrode is removed from the electrochemical cell at a specified potential. The return to the vacuum is facilitated by the use of completely volatilizable electrolytic solutions such as HF dissolved in water. Otherwise, the electrode surface must be rinsed free of electrolyte with solvent, and this invites structural and chemical changes. With metal electrode surfaces on which the solution exhibits a high contact angle, it is possible to emerse the surface from the solution with only adsorbed species and a very thin layer of solution retained on the surface. Using a metal such as gold, the residual electrolyte layer may be equivalent to such a small fraction of a monolayer that post-electrochemical examination is possible even with a non-volatilizable electrolyte after removal of the solvent by volatilization. Such transfers are feasible only for single crystal studies of metal which are relatively noble in the particular electrolytic solution: for example, platinum, gold, and silver in aqueous solutions. More active metals will react with the solution upon loss of the potential control when the electrode is withdrawn from the electrochemical cell.

Research groups involved in such experiments in the U.S. include those of Professor A. Hubbard[35, 36] at the University of Santa Barbara, Dr. Philip Ross[37] at the Lawrence Berkeley Laboratory, Dr. W. E. O'Grady at Brookhaven National Laboratory, Dr. J. A. Joebstl[38] at Fort Belvoir and the authors' research groups[39-41].

The Ultrahigh Vacuum—Electrochemical System at Case Western Reserve University

The system in use in the authors' laboratories was initially designed in 1975 by Dr. O'Grady (now at Brookhaven National Laboratory) together with two of the authors (BDC, EY). Since then, the system has further evolved through the efforts of several former graduate students including Drs. M. Woo (now at Engelhart Industries), P. Hagans (Dow Chemical Co) and A. Homa (General Electric's Nela Park Laboratory) and one of the authors (MH). A schematic diagram is shown in Figure 16. High quality single crystal surfaces are prepared and cleaned up by standard techniques. The usual procedure with metals such as platinum and gold is to repeatedly argon ion sputter and thermally anneal the crystal so as to allow impurities to diffuse to the surface and be removed. The quality of the surface is examined with LEED in the right hand Chamber A in UHV (5×10^{-11} Torr). The surface is checked for impurities with AES and also XPS. The single crystal electrode is then trans-

ferred into the left hand vacuum Chamber B by means of a magnetically coupled manipulator without loss of UHV integrity. Ultrapure argon is then admitted to Chamber B, and an electrochemical cell is formed by bringing up a counter electrode with its surface parallel to that of the single crystal electrode. A drop of solution is applied to the horizontal surface of the counter electrode and then squashed between the single crystal and counter electrode. In recent work with this system, a third wire electrode ($\alpha-$ Pd/H) has been placed between the two parallel electrode surfaces and used as a reference. Following the electrochemical measurements, the single crystal electrode and the counter electrode are separated and the solution removed usually by volatilization. In some instances, the single crystal electrode surface is wiped free of bulk solution before volatilization of the residual subsolution layer. The pressure in Chamber B is then rapidly pumped down to 10^{-7} Torr, and the sample retransferred back into Chamber A through the low conductance gate valve. The surface is then examined with LEED, XPS, and AES at a pressure of 10^{-10} Torr in a time as short as 6 minutes following the separation of the single crystal and counter electrodes.

Figure 16

Apparatus for single crystal electrochemical studies using LEED, Auger electron spectroscopy and x-ray photoelectron spectroscopy at CWRU (M. Hanson[42]).

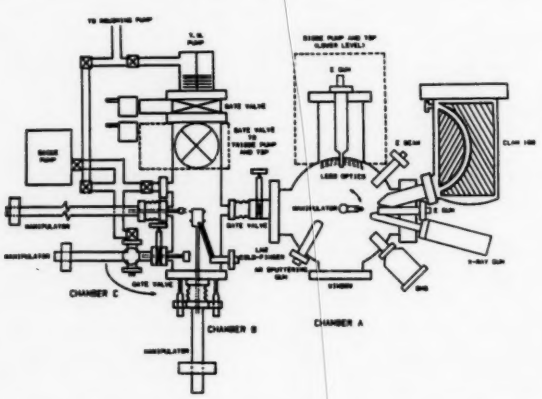

Figure 17

Three electrode system used at CWRU for LEED-AES-XPS studies of hydrogen adsorption on single crystal platinum electrodes (M. Hanson[42]).

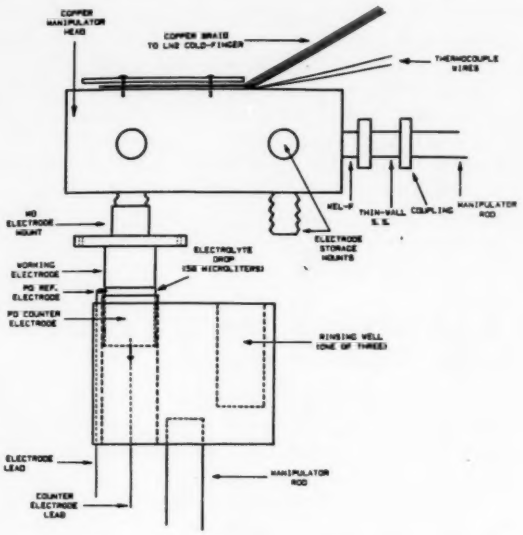

Studies of Underpotential Deposition on Single Crystal Surfaces

The CWRU group has used its transfer system to examine the underpotential deposition of lead on the low index single crystal surfaces of gold[40] and silver.[41] A lead counter electrode was used for the former with the counter electrode also used as the reference; while for the latter a three-electrode cell was used as described earlier with the counter electrode palladium charged with hydrogen and the reference electrode a lead wire.

The voltammetry curves for lead UPD on the three low index surfaces of silver (shown in Figure 18) are typical of the results obtained for UPD on various single crystal metals. These curves indicate multiple peaks even on the low index silver surfaces. These electrodes have been removed from the electrochemical environment at various potentials in the UPD range and reexamined with LEED, AES, and XPS. Intriguing LEED patterns have been obtained[42] at various coverages indicating various types of ordering phenomena. These account for this complex form of the voltammetry curves.

Figure 18a

Voltammorgram of Ag(111) in 0.1 *M* HF and 3×10^{-3} *M* PbF_2. First sweep, sweep rate = 10 mV/s. Cell formed under potential control at 0.4 V.

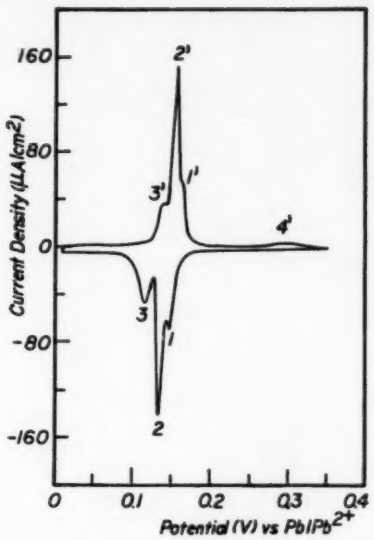

Figure 18b

Voltammogram of Ag(110) in 0.1 *M* HF and 3×10^{-3} *M* PbF_2. First sweep, sweep rate = 10 mV/s. Cell formed at 0.3 V.

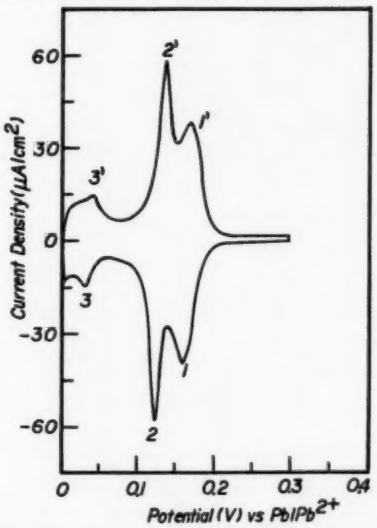

Figure 18c

Voltammogram of Ag(100) in 0.1 *M* HF and 3×10^{-3} *M* PbF_2. First sweep, sweep rate = 20 mV/s. Cell formed under potential control at 0.4 V.

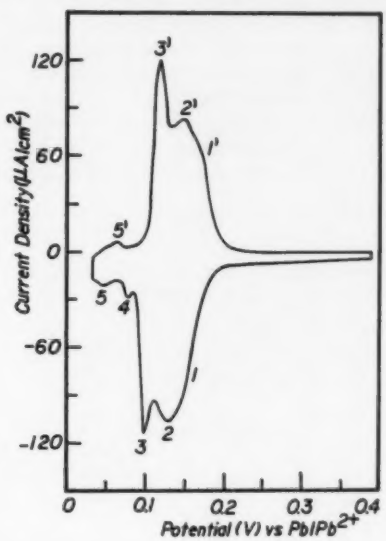

Studies of Hydrogen Adsorption on Single Crystal Platinum Surfaces

The voltammetry curves for H adsorption—desorption on the low index surfaces of platinum are shown in Figure 19. The potential sweeps have been restricted to the indicated potential region. Sweeping to more anodic potentials where anodic film formation occurs results in major changes in the H adsorption region. This is believed to be caused by restructuring of the platinum single crystal surfaces at the more anodic potentials. These voltammetry curves compare favorably with those obtained by Dr. P. Ross and his research group at the Lawrence Berkeley Laboratory. The platinum single crystals used by both groups were aligned and polished by Dr. W. Heppler of the Lawrence Berkeley Laboratory. The etching of surfaces and final clean up and annealing of the crystals were done individually by the Berkeley and CWRU groups. The surfaces were subjected to from 10 to 15 cycles of argon ion sputtering and high temperature annealing to remove impurities including carbon and to achieve surfaces yielding high quality LEED patterns. The (111) surface shows a very broad peak with some evidence of fine structure while one predominant peak is evident in the (110) and (100) surface with two smaller peaks also evident on the (100) surface. These voltammetry curves indicate that the single crystal substrates have a strong influence on the hydrogen adsorption-

desorption, but that even on a low index surface the behavior is still rather complex. Platinum single crystals with their surfaces finished off in slightly different ways, however, have yielded different hydrogen adsorption-desorption voltammetry curves, particularly for the (100) surface even though the LEED patterns before and also after the electrochemical measurements are very similar.

This type of research is still in an early stage where the possibility of artifacts and even impurity effects can not be ruled out. Nonetheless, it is essential that such studies be carried out if electrochemists are to gain insight as to the role of surface morphology in electrocatalysis. Over the coming decade, much progress is expected.

Figure 19a

First three voltammetry curves on Pt(111) in 0.1 *M* HF. Immersion potential = 0.55 V. Sweep rate = 50 mV/s.
——— = first sweep.
•••• = second sweep.
---- = third sweep.
Integration of cathodic region on first sweep = −139 C/cm².

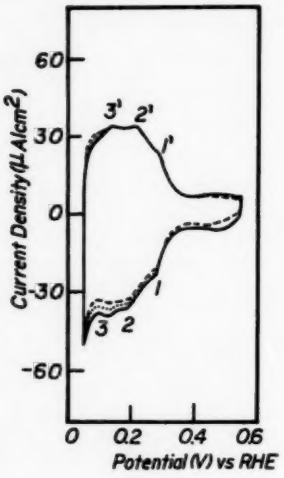

Figure 19b

Voltammetry curves of Pt(110) in 0.1 *M* HF. Immersion potential = 0.55 V, first sweep cathodic to 0.45 V. Cathodic limit opened in 50 mV increments on each successive sweep. Sweep rate = 50 mV/s.

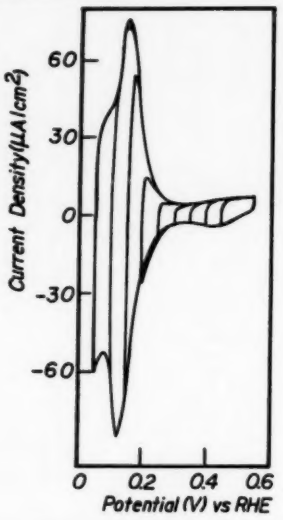

Figure 19c

Voltammetry curves of Pt(100) in 0.1 *M* HF. Immersion potential = 0.55 V. Sweep rates = 20, 50, 100 mV/s.

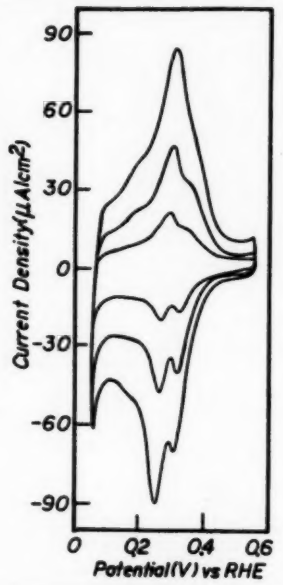

References

1. Yeager, E., "Non-Traditional Approaches to the study of Solid-Electrolyte Interfaces: Problem Overview," *Surface Science 101* (1980) pp. 1-22.

2. O'Grady, W.E., M.Y.C. Woo, P.C. Hagans and E. Yeager, *Electrode Materials and Processes for Energy Conversion and Storage*, J.D.E. McIntyre, S. Srinivasan and F. G. Will, eds., The Electrochemical Society, Pennington, N.J. (1977) p. 172-184.

3. Otto, A., "Excitation of Nonradiative Surface Plasma Waves in Silver by the Method of Frustrated Total Reflection," *Zeitschrift fur Physik, 216* (1968) p. 398.

4. Kretschmann, E., and H. Raether, "Radiative Decay of Nonradiative Surface Plasmons Excited by Light," *Zeitschrift fur Naturforsch, 23A* (1968) p. 2135.

5. Gordon, J. and S. Ernst, "Surface Plasmons as a Probe of the Electrochemical Interface," *Surface Science, 101* (1980) pp. 499-506.

6. Nikolic, B.Z., R.R. Adzic and E. Yeager, "Reflectance Spectra of Monolayers of Tetrasulfonated Transition Metal Phthalocyanines Adsorbed on Electrode Surfaces,"*Journal of Electroanalytical Chemistry, 103* (1979) pp. 281-287.

7. Adzic, R., E. Yeager and B.D. Cahan, "Optical and Electrochemical Studies of Underpotential Deposition of Lead on Gold Evaporated and Single Crystal Electrodes," *Journal of Electrochemical Society 121* (1974) pp. 474-484.

8. Adzic, R., B.D. Cahan and E. Yeager, "Complex Plane Analysis in Electrode Modulated Specular Reflectance Studies, *Journal of Chemistry and Physics 58* (1973) pp. 1780-1782.

9. Cahan, B.D. and R.F. Spanier, *Surface Science, 16* (1969) p. 166.

10. Cahan, B.D., "Implications of the Three Parameter Solutions to the Three-Layer Model," *Surface Science, 56* (1976) p. 354.

11. Reed, A. and E. Yeager, "The Effect of Optical Polarization on Reflection Spectra," *Reflection of Applied Optics 7* (1968) p. 451.

12. Reed, A. and E. Yeager, "Infrared Internal Reflection Studies of the Germanium/Electrolyte Interface," *Electrochimica Acta 15* (1970) pp. 1345-1354.

13. Bewick, A., K.K. Kunimatsu and B.S. Pons, *Electrochimica. Acta 25* (1980) p. 465.

14. Bewick, A., "*In-situ* Infrared Spectroscopy of the Electrode/Electrolyte Solution Interphase," *Journal of Electroanalytical Chemistry 150* (1983) pp. 481-493.

15. Pons, S., "The use of Fourier transform Infrared Spectroscopy for *in situ* Recording of Species in the Electrode-Electrolyte Solution interphase," *Journal of Electroanalytical Chemistry 150* (1983) pp. 495-504.

16. Bewick, A., K.K. Kunimatsu, J. Robinson and J.W. Russell, "IR Vibrational Spectroscopy of Species in the Electrode-Electrolyte Solution Interface," J. Electroanalytical Chemistry 119 (1981) p. 175.

17. Neugebauer, H., G. Nauer, N. Brinda-Konopik and G. Gidaly, "The *in-situ* Determination of Oxidation Products on Iron Electrodes in Alkaline Electrolytes Using Multiple Internal Reflection Fourier Transform Infrared Spectroscopy," *Journal of Electroanalytical Chemistry, 122* (1981 p. 381.

18. Fleischmann, M., P.J. Hendra and A.J. McQuillan, *Journal of Chemical Society and Chemical Communication, 3* (1973) p. 80; see also Chem. Phys. Lett., *26* (1974) p. 163.

19. McQuillan, A.J., P.J. Hendra and M. Fleischmann, *Journal of Electroanalytical Chemistry, 65* (1975) p. 933.

20. Jeanmaire, D.L. and R. P. Van Duyne, *Journal of Electroanalytical Chemistry 84* (1977) 1; see also R.P. Van Duyne, (C5) *Journal de Physique, Colloque* (1977) pp. 239-252.

21. Furtak, T.E., "Current Understanding of the Mechanism of Surface Enhanced Raman Scattering," *Journal of Electroanalytical Chemistry, 150* (1983) pp. 375-388.

22. Campion, A. and D.R. Mullins, "Normal Raman Scattering from Pyridine Adsorbed in the Low Index Faces of Silver," *Chemistry and Physics Letter 94* (1983) pp. 576-579; see also A. Campion, V.M. Grizzle, D.R. Mullins and J.R. Brown, (C10) *Journal de Physique, Colloque* (1983) pp. 341-344.

23. Simic-Glavaski, B., S. Zecevic and E. Yeager, "Spectroscopic and Electrochemical Studies of Transition Metal Tetrasulfonated Phthalocyanines," *Journal of Physical Chemistry, 87* (1983) pp. 4555-4557; see also *Journal of Electroanalytical Chemistry, 150* (1983) 469-479.

24. Brazdil, J.F., and E. Yeager, "Resonant Raman Spectra of Adsorbed Species at Solid-Gas Interfaces," *Journal of Physical Chemistry, 85* (1981) pp. 995-1004; see also ibid., 85 (1981) pp. 1005-1014; ibid., *85* (1981) pp. 2194-2199.

25. Kotz, R. and E. Yeager, "Raman Studies of the Silver-Silver Oxide Electrode, *Journal of Electroanalytical Chemistry, 111* (1980) pp. 105-110.

26. Kotz, R. and E. Yeager, Potential Dependence of Vibrational Frequencies of Adsorbates on a Silver electrode, *Journal of Electroanalytical Chemistry, 123* (1981) pp. 335-344.

27. Anderson, A.B., R. Kotz and E. Yeager, Theory for CN^- and Ag – C Vibrational Frequency Dependence on Potential; Cyanide on a Silver Electrode, *Chem. Phys. Lett. 82* (1981) pp. 130-134.

28. O'Grady, W.E., "Mossbauer Study of the Passive Oxide Film on Iron," *Journal of Electrochemical Society, 127* (1980) p. 555.

29. Eldridge, J., M.E. Kordesch and R.W. Hoffman, *J. Vac. Sci. Technol. 20* (1982) p. 934.

30. M.E. Kordesch, J. Eldrige, D. Scherson and R.W. Hoffman, A New Mossbauer Conversion Electron Detection Technique for *in situ* Passivation Studies on Iron, *Journal of Electroanalytical Chemistry, 164* (1984) p. 393.

31. Chen, C.T., and B.D. Cahan, *Journal of Electroanalytical Chemistry Society, 129* (1982) p. 17.

32. Kuroda, K., B.D. Cahan, G. Nazri, E. Yeager and T.E. Mitchell, "Electron Diffraction Study of the Passive Film on Iron," *Journal Electrochemistry Society 129* (1982) pp. 2163-2169.

33. Scherson, D., C. Fierro, E. Yeager, M.E. Kordesch, J. Eldridge, R.W. Hoffman and A. Barnes, "*in situ* Mossbauer Spectroscopy on an Operating Fuel Cell," *Journal Electroanalytical Chemistry 169* (1984) pp. 287-302; see also D. Scherson et al., *Journal of Physics and Chemistry, 87* (1983) pp. 932-943.

34. Fine, J.M., J.J. Rusek, J. Eldridge, M.E. Kordesch, J.A. Mann, R.W. Hoffman and D.R. Sandstrom, *Journal of Vacuum Science and Technology, 1A* (1983) pp. 1036-1038.

35. Ishikawa, R.M. and A.T. Hubbard, *Journal of Electroanalytical Chemistry, 69* (1976) p. 317.

36. Hubbard, A.T., R.P. Ishikawa and J. Katekaru, *Journal Electroanalytical Chemistry, 86* (1978) p. 271.

37. (A) Ross, P.N., "The Effect of Air Ions on Hydrogen Chemabsorption and Oxide Formation on PT in Equious Acids," *Journal of the Electro-analytical Chemistry, 76* (1977) p. 139.

(B) Ross, P.N., "Structure Sensativity in the Electrocatalytic Properties of P.T.," *Journal of the Electrochemical, 126* (1979) p. 67.

38. Joebstl, J.A., "Surface Characterization of Electrocatalysts by LEED, Auger Electron Spectroscopy and Related Techniques," First Chemical Congress of the North American Continent, Mexico City, November 30-December 5, 1975, Abstract PHSC-18.

39. O'Grady, W.E., M.Y.C. Woo, P.L. Hagans and E. Yeager, Electrode Materials and Processes for Energy Conversion and Storage, J.D.E. McIntyre, S. Srinivasan and F.G. Will, eds., (Electrochemical Society, Pennington, N.J., 1977).

40. Yeager, E., A. Homa, B.D. Cahan and D. Scherson, "Spectroscopic Techniques for the Study of Solid-Liquid Interfaces," *Journal of Vacuum Science and Technology, 20* (1982) pp. 628-634.

41. Homa, A.S., E. Yeager and B.D. Cahan, "LEED-AES Thin-Layer Electrochemical Studies of Hydrogen Adsorption on Platinum Single Crystals," *Journal of Electroanalytical Chemistry, 150* (1983) pp. 181-192.

42. Hanson, M. *Ph.D. thesis*, Chemistry Department, Case Western Reserve University, Cleveland, Ohio, 1985.

Biography

Dr. Ernest Yeager is Hovorka Professor of Chemistry and Chemical Engineering at Case Western Reserve University, Cleveland, Ohio. For many years, he has been a principal investigator for the Office of Naval Research. His research has been in electrochemistry, primarily in the area of electrocatalysis and electrolytes. At Case Western, Dr. Boris Cahan is a Professor of Chemistry, Dr. Daniel Scherson is an Assistant Professor of Chemistry, and Dr. Michael Hanson was a graduate student.

HIGH CONDUCTIVITY SOLID ELECTROLYTES: A REVOLUTION IN SOLID STATE CHEMISTRY

By Gregory C. Farrington, University of Pennsylvania and Bruce Dunn, University of California, Los Angeles

Introduction

High conductivity solid electrolytes are remarkable solids that have ionic conductivities comparable to liquid electrolytes. They include elegant crystalline compounds, amorphous glass compositions, and polymer complexes. They have revolutionized electrochemistry in the past twenty years and are now being applied in a new generation of solid state sensors and high energy density storage batteries. Recent discoveries have shown that their potential applications also include various opto-electronic devices. One specific family of solid electrolytes may be of considerable interest as new laser and phosphor hosts.

Although major scientific and technological interest in high conductivity solid electrolytes is recent, the earliest examples of such materials were reported in the 1800's by two giants of the field of chemistry, Michael Faraday and H.W. Nernst.

In 1837, Faraday found that PbF_2 at red heat has an electrical conductivity comparable to metals. Yet, PbF_2 is an electronic insulator. Nernst, around the turn of the century, studied the ionic conductivity of various inorganic oxides. His famous Nernst lamp, the heart of which was a small cerium oxide rod heated by a current of oxygen ions, was an early example of a technology that used solid ionic conductors. It was a contender for practical electric lighting. It ultimately lost out to the simpler and cheaper light bulb based on Thomas Edison's designs and made practical by Coolidge's development of a method for drawing fine tungsten filaments and Irving Langmuir's early studies of hot filaments in gas-filled glass tubes.

We now know that the high electrical conductivity of PbF_2 results from the motion of ions, not electrons. Fluoride ions in PbF_2 diffuse rapidly through the structure around essentially-immobile lead cations. Similarly, in cerium oxide and related compounds, oxygen ions diffuse rapidly at high temperatures.

Many other compounds and solid compositions with high ionic conductivities have since been discovered. They range from $RbAg_4I_5$, which has a conductivity for Ag^+ ions at 25°C that is comparable to aqueous electrolytes, to Nd^{3+} beta" alumina, which has a relatively high ionic conductivity for Nd^{3+} above about 500°C. Conductors exist for a large fraction of the monovalent, divalent, and trivalent cations in the periodic chart, and also for selected anions, such as O^{2-}, F^-, and ClO^{4-} (Table 1).

Table 1

Representative Solid Electrolytes

Compound	Mobile Ion
AgI	Ag^+
$RbAg_4I_5$	Ag^+
Li_3N	Li^+
$Na_3Zr_2PSi_2O_{12}$	Na^+
$HUO_2PO_4.4H_2O$	H^+
Beta'' Alumina	Na^+, K^+, Ag^+, Ca^{2+}, Sr^{2+}, Ba^{2+}, Pb^{2+}, Hg^{2+}, Cd^{2+}, Zn^{2+}, Mn^{2+}, Eu^{2+}, Sm^{2+}, Nd^{3+}, and other trivalent, lanthanides and, bivalent cations
$CaO.ZrO_2$	O^{2-}
PEO complexes	Li^+, Na^+, K^+, SCN^-, ClO_4^-, and other trivalent lanthanides and divalent cations

How Do Solids Conduct Ions?

The classic mechanisms by which solids conduct ions were first described by Frenkel and Schottky in the early 1900's. Frenkel noted that, if an ion in a normal lattice position moves to an interstitial site, it leaves behind a vacancy and can then hop to an adjacent interstitial site or vacant lattice site. In this way, the ion and its charge are transported through the solid structure. Schottky proposed a slightly different mechanism. He suggested that a small fraction of normal lattice sites can be unfilled by their appropriate ions. The resulting vacancies can move through the structure and transport charge (Figure 1).

Figure 1

Frenkel (interstitial) and Schottky (vacancy) defects in a crystalline solid. All real ionic crystals have a population of these defects, which can produce ionic conductivity in the solid state.

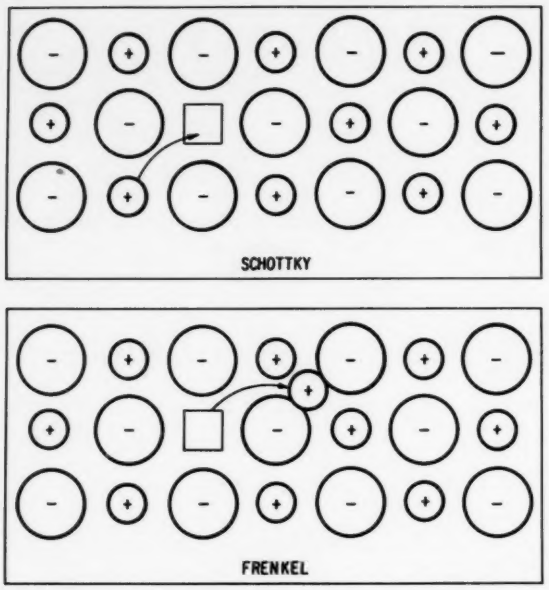

Thermodynamics tell us that all ionic solids at 0 °K have a statistical population of Frenkel and Schottky defects. Frenkel defects are more common in some compounds, such as the silver halides, and Schottky defects in others, such as the alkali halides. In any specific compound, the fraction of ions 'out of place' depends on the energy required to create the defects. The rate at which these ions or defects diffuse through a particular compound determines its ionic conductivity and depends upon the energy required to move an ion from one interstitial site to another or from a filled lattice site to a vacancy.

For normal compounds, the energy required to create defects is rather high, typically 1-2 eV. As a result, the defect population is small. For example, the fraction of Schottky-type defects (vacancies) in NaCl at 25 °C is only about 10^{-17}, and only 10^{-5} at 800 °C, one degree below its melting point. The ionic conductivity of NaCl is correspondingly low, less than 10^{-8} $(\text{ohm-cm})^{-1}$ at 250 °C.

However, in some rare compounds, the energy of defect creation is nearly zero. One example, is alpha AgI, which exists above 147 °C. This material consists of Ag^+ ions in tetrahedral sites in a body-centered-cubic array of I^- ions. There are several times the number of tetrahedral sites as Ag^+ ions. In fact, the Ag^+ ions are not located in a specific subset of tetrahedral sites, but are disordered among all of the tetrahdral sites. As a result, AgI has an ionic conductivity for Ag^+ of about 10^- $(\text{ohm-cm})^{-1}$ at 160 °C. Ag^+ ions are so conductive in solid AgI that its conductivity actually decreases when it melts. Most salts have conductivities 10^4-10^5 times greater in the molten state than in the crystalline state.

The characteristics that produce high ionic conductivity in AgI or in any other solid are the same. For a solid to be a good ionic conductor, it first must have a population of ions distributed among a larger group of vacant sites. In addition, the energy required to disorder the ions among the vacant sites (the energy of defect creation), and the energy required to move ions among the sites (the energy of defect migration) must be small.

Typical High Conductivity Solid Electrolytes

High conductivity solid electrolytes range from crystalline materials with well-defined structures (the stabilized zirconias (e.g., $xCaO.ZrO_2$), the beta'' aluminas ($Na_{1.67}Mg_{0.67}Al_{10.33}O_{17}$), and $RbAg_4I_5$) to amorphous glasses and soft polymers (the ionically-conductive complexes formed between polyethylene oxide (PEO) and various alkali ion salts). Typical solid electrolytes are electronic insulators, although some, termed ion insertion compounds, have both electronic and ionic conductivity. Most solid electrolytes conduct one specific ion. A few, such as the beta aluminas, host the diffusion of many different cations. Some solid electrolytes conduct in only one direction, by ion motion down atomic-level tunnels. Others conduct in two dimensions with ion diffusion in open planar regions. Still others conduct in all three dimensions. This anisotropy of ionic diffusion is one characteristic that is peculiar to solid electrolytes and distinguishes them from liquid electrolytes.

The remainder of this article presents brief descriptions of several specific groups of solid electrolytes and their potential technological applications.

The Stabilized Zirconias—Materials for High Temperature Sensors

Oxygen ions diffuse slowly in most solid oxides. However, at temperatures of 500-1000 °C, various solid solutions formed by Group IVB oxides (such as ZrO_2 and HfO_2) and ThO_2 with CaO and Y_2O_3 are unusually-conductive solid electrolytes for oxygen ions. They are widely used as electrolytes in oxygen sensors for automotive and industrial combustion conotrol and also in experimental high temperature fuel cells.

These high conductivity solid electrolytes have the fluorite crystal structure, which is a face-centered-cubic

arrangement of cations with the oxide ions occupying the tetrahedral sites. In ZrO_2, for example, all of the tetrahedral sites are filled by oxygen ions. But, by partially substituting Ca^{2+} for Zr^{4+} in the structure, compensating vacancies are created in the oxygen sites, which give rise to rapid oxygen ion motion at high temperatures. The additional CaO also stabilizes the crystal structure in the conductive fluorite form. Normally, ZrO_2 is stable in the fluorite structure only above about 2300 °C. At lower temperatures, it forms other structures. With the addition of CaO, the fluorite structure is stable at temperatures as low as 800-1000 °C. The resulting solid solutions are referred to as calcia-stabilized zirconia (CSZ). Similar structures occur with solid solutions of Y_2O_3 in ZrO_2, as well as CaO and Y_2O_3 in ThO_2 and HfO_2.

The conductivity of CSZ is actually quite low at ordinary temperatures. It is estimated to be less than 10^{-16} $(ohm\text{-}cm)^{-1}$ at 25 °C, and varies with an activation energy of about 1-1.5 eV. These values are similar to those observed for ionic transport in such classical compounds as the alkali halides. As a result, these oxygen ion conductors are not in the same class as electrolytes, that have high ionic conductivities at 25-100 °C, such as $RbAg_4I_5$ and the beta aluminas.

However, the stabilized oxide electrolytes have such high melting points that they can be heated to temperatures at which they develop high conductivities. Their high melting points distinguish them from compounds such as NaCl and LiI which melt long before they become good conductors. Regardless of their strict classification among solid electrolytes, the oxide electrolytes are good conductors under specific circumstances and have found considerable technological application.

The most widespread use of these materials is as electrolytes in sensors for automotive combustion control. Virtually all new cars sold in the United States incorporate one of these devices as part of a carburation control system to help increase gas mileage and control pollution. Another application is in oxygen sensors for steelmaking. A major application of these materials that is still in the research and development stage is in high temperature fuel cels. Active development efforts in this area are underway at the research laboratories of the Westinghouse Corporation and elsewhere.

Ion Insertion Compounds—Revolutionary Electrode Materials for Batteries

Some solid electrolytes are also good electronic conductors. This makes them particularly useful as electrode materials in batteries. These materials, which include both inorganic and organic substances, are generally referred to as ion insertion compounds.

TiS_2 is the archetype ion insertion compound. Its structure, shown in Figure 2, consists of strongly-bonded TiS_2 layers, bounded by sheets of close-packed sulfur atoms. The sulfur sheets are held together by weak van der Waal's forces.

Pure TiS_2 is a semiconductor. It also can be chemically or electrochemically reduced as in Reaction 1.

$$TiS_2 + ne^- + nM^+ = M_nTiS_2 \text{ (Rxn. 1)}$$

M can be various monovalent cations, but is commonly Li^+. As the reduction proceeds, the cations intercalate between the weakly-bonded layers of sulfur atoms. The structure swells in proportion to the cation size in order to accommodate the ion insertion.

Figure 2

Structure and intercalation reaction of TiS_2.

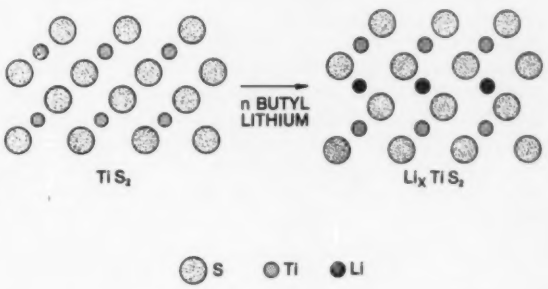

The ion insertion reactions are generally reversible within a certain composition range. For example, Li_xTiS_2 can be cycled from $x = 0$ to $x = 1$ hundreds of times. This electrochemical reversibility is one reason why $LiTiS_2$ and similar compounds are so interesting as electrodes for energy storage in batteries. However, for any particular ion insertion compound to be truly useful as a battery electrode, the free energy of the reduction process (Rxn. 1) and the maximum intercalation level, x, must be as high as possible.

Many compounds have been discoverred which meet all of these conditions. Included are layer compounds (TiS_2, VS_2), in which ion diffusion is two-dimensional, chain compounds (NbS_3, TiS_3), in which ion insertion is quasi-one-dimensional along molecular chains, and framework structures (MnO_2 WO_3, and V_6O_{13}), which support ion diffusion in three dimensions within an oxide framework. It is appropriate to include among these compounds the recently-discovered polymer electrodes, such as polyacetylene $(CH)_x$ and related compounds, which undergo similar ion-insertion reactions. Polyacetylene can be both reduced and oxidized with the

insertion of either cations or anions, as shown in Reactions 2 and 3. The various reduced and oxidized polyacetylenes and similar compounds are of some interest as electrode materials in electrochemical systems.

$$(CH)_x + yM^+ + ye^- = (M_yCH)_x \text{ (Rxn. 2)}$$

$$(CH)_x + yX^- = (CHX_y)_x + ye^- \text{ (Rxn. 3)}$$

The most promising ion insertion compounds for use in batteries are TiS_2 and V_6O_{13}. These compounds have been widely investigated as positive electrodes in rechargeable high energy density batteries that can store 5-10 times the energy of a conventional nickel-cadmium battery. Lithium is the typical negative electrode for these batteries. Because the high energy electrodes would react with conventional aqueous electrolytes, the batteries require non-aqueous or solid electrolytes for their operation.

A principal technological goal of this work is the development of a battery for electric cars. A great deal of research has been carried out in this area over the past 15 years. But, the problems of dealing with high energy electrodes, non-aqueous electrolytes, and the stringent demands of the electric vehicle application are formidable. No rechargeable battery using a non-aqueous liquid electrolyte has yet been commercialized. Interestingly, one of the most promising batteries of this type uses a solid polymeric ionic conductor discussed in the next section.

Polymeric Solid Electrolytes— Thin Film Electrolytes for Batteries

Some of the most intriguing solid electrolytes investigated over the past ten years are not truly solids, but are amorphous polymer complexes. These materials can be simply cast as thin polymer films. The processes by which they conduct ions are similar to those in liquid electrolytes. Yet, unlike hard, crystalline electrolytes, they can flow under stress. The ability to deform makes them extremely promising electrolyte materials for use in a remarkable high energy density, all-solid-state battery.

The materials which stimulated interest in polymer solid electrolytes are the complexes formed by polyethylene oxide and various alkali ion salts, such as LiSCN, NaI, and $LiClO_4$. The polymer electrolytes can be formed simply by dissolving the polymer and the salt in a mutual solvent and evaporating the solution on a smooth plate. The result is a thin polymeric film which can contain both crystalline and amorphous compositions of the type, $(PEO)_xLiClO_4$, as well as uncomplexed salt and polymer. The specific phases present depend on the salt/polymer ratio and the temperature.

The polymer complex films have reasonable ionic conductivities for both cations and anions. The fraction of charge carried by each depends on the specific salt in the complex and on other factors such as temperature. Recent research indicates that ionic conductivity takes place principally in the amorphous complex phase, which behaves like an extremely viscous liquid electrolyte. A typical film of a PEO-$LiClO_4$ complex has a conductivity of 10^{-4} (ohm-cm)$^{-1}$ at 60°C. Many other compositions have been synthesized.

These materials are lower in conductivity than many crystalline conductors. However, unlike crystalline materials, they can be easily formed into thin films, which, because the polymer can flow, may make it possible someday to power electric cars with a high energy density, rechargeable battery that uses no liquid electrolytes and is truly all-solid-state.

The particular attractiveness of the all-solid design is that it minimizes the volume and weight of the electrolyte. Although the electrolyte is essential, it takes up weight and space that might otherwise be devoted to the active electrodes, and therefore reduces the energy stored per unit weight and volume.

An all-solid-state battery using polymer electrolytes (Figure 3) is already being developed at several laboratories in France, Canada, England, and the United States. Lithium or a lithium alloy is used as the negative electrode and an ion insertion compound, such as TiS_2 or V_6O_{13}, as the positive electrode. When the battery is discharged, lithium is oxidized at the lithium/ polymer interface, transported as Li^+ across the membrane, and inserted into the TiS_2, which is reduced. The process is reversed when the cell is recharged.

The chief difficulty in making a successful solid state battery stems from the unavoidable transport of ions from one electrode to the other. The oxidation of lithium, for example, strips lithium away from the interface. Unless the interface can deform so that lithium/electrolyte contact is maintained, the battery stops working. Similarly, the insertion of Li^+ into TiS_2 swells the TiS_2 and jeopardizes contact at that interface.

Many all-solid-state batteries using hard, crystalline solid electrolytes have been proposed. But, they have all founded on the problem of maintaining interfacial contact as the battery is discharged. The special feature of the polymer electrolytes is that they can flow, thus interfacial contact in batteries of the type shown in Figure 3 is maintained at reasonable current densities. Development efforts on systems of this sort are moving from the research to the prototype stage. Many difficulties remain. Initial performance indicates that, if laboratory cells can be successfully scaled-up, real solid state polymeric batteries would be able to store more than five times the energy per unit weight and volume as conventional lead-acid ('car') batteries and deliver the energy at the rates needed for powering an automobile.

Figure 3

An all solid state electrochemical cell. Li and V_6O_{13} are the electrodes. They are embedded in conductive polymer and separated by a thin sheet of conductive polymer.

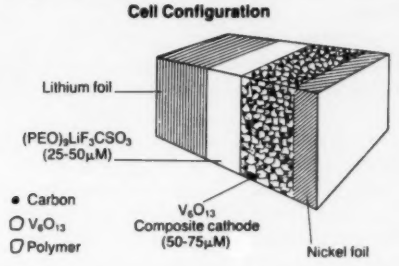

Beta Aluminas— New Laser and Phosphor Hosts

The beta aluminas are perhaps the most widely-investigated family of solid electrolytes. The beta and beta" alumina structures are unique among solid electrolytes in that they host the rapid diffusion of many different cations: movovalent, bivalent, and trivalent. This gives them a richness of chemistry and breadth of application unmatched by any other solid electrolyte.

In reality, the terms beta and beta" alumina are misnomers. Both compounds are actually non-stoichiometric sodium aluminates which can be considered derivatives of an unreported ideal composition, $NaAl_{11}O_{17}$. Typical compositions are $Na_{1.2}Al_{11}O_{17.1}$ for sodium beta alumina and $Na_{1.67}Mg_{0.67}Al_{10.33}O_{17}$ for sodium beta" alumina. Both electrolytes are layer structures in which ionic diffusion occurs in two-dimensional conduction planes [Figure 4].

Sodium beta alumina has been known since about 1916. It has long been sold as a refractory brick material for constructing high temperature furnaces. In 1965, researchers at the Ford Motor Company Research Laboratories discovered that it has a sodium ion conductivity at room temperature comparable to that of an aqueous sodium chloride solution. Their findings focused attention on the science and technology of high conductivity solid electrolytes.

Most of the technological development of sodium beta/beta" alumina has been directed toward a revolutionary electrochemical system, the sodium/sulfur battery, which uses a polycrystalline ceramic membrane of sodium beta/beta" alumina to separate molten sodium and molten sulfur electrodes (Figure 5). The battery, which has liquid electrodes and a solid electrolyte, is the inverse of traditional batteries, which have solid electrodes and liquid electrolytes. If successfully developed, it will be a candidate for powering electric cars.

However, the most exciting potential applications of beta and beta" alumina may be in technologies that are far from electrochemical energy storage. The new areas of application are in phosphors, lasers, and integrated optics. They have grown from the discovery that it is possible to replace the entire Na^+ content of beta" alumina with divalent and trivalent cations in simple ion exchange reactions.

Figure 4

Structure of sodium beta" alumina shown edge-on. Ionic conduction occurs in relatively-open planes perpendicular to the page and marked by the sodium ions.

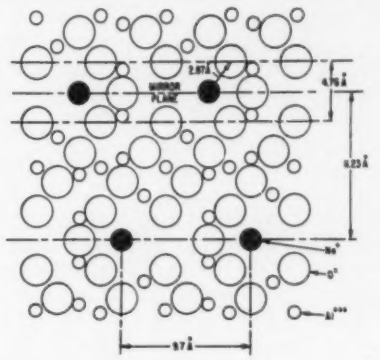

Figure 5

Sodium/sulfur battery. The liquid sodium and sulfur electrodes are separated by a thin tube of polycrystalline sodium beta or beta" alumina. The cell functions at 300-350 °C.

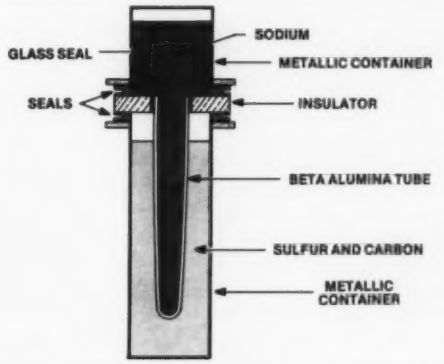

It has long been known that the sodium ions in both beta and beta" alumina can be exchanged with other monovalent cations such as Ag^+, K^+, and Li^+. The process is quite simple. When, for example, a crystal of

sodium beta alumina is immersed in molten KNO_3 at 350°C, within minutes all of the sodium ions diffuse out and are replaced by potassium ions. About 15 years ago, similar experiments were tried with sodium beta alumina and various molten bivalent cation salts. Very little ion exchange took place, which discouraged interest in attempting to make solid electrolytes for polyvalent cations.

However, recent discoveries have shown that although bivalent and trivalent cations diffuse very slowly in beta alumina, they exchange rapidly with the sodium content of beta" alumina. It is possible to prepare derivatives of beta" alumina in which the sodium ion content has been replaced by Ca^{2+}, Ba^{2+}, Cd^{2+}, Nd^{3+}, Eu^{3+}, Er^{3+}, and many other bivalent and trivalent cations. The bivalent and trivalent beta" aluminas are the first general family of solid electrolytes for polyvalent cations. They demonstrate that the phenomenon of rapid ion transport in solids is not limited to a few monovalent cations, but occurs quite generally with many of the elements of the periodic chart.

The most exciting polyvalent beta" aluminas are those that contain lanthanide ions (see cover picture). Nd^{3+} beta" alumina has already been shown to support both pulsed and cw laser action. Its applications as a new laser host material for Nd^{3+} are being actively studied in several laboratories. Because the Nd^{3+} ions are diffused into the beta" alumina crystals after they are grown, the processes of crystal growth and doping are separate. Therefore it is possible, at least conceptually, to prepare specific spatial distributions of the active ions as well as unusual combinations of lanthanide ions by simple diffusion processes. This capability is unique among laser hosts. Research on the optical applications of the lanthanide beta" aluminas is only beginning. It will be several years before their properties and possibilities are understood.

Conclusions

The observation that ions diffuse rapidly in certain solids is not new. It can be traced back to Faraday and Nernst. However, early solid electrolytes were solid state curiosities. They either conducted at very high temperatures (the zirconias and related compounds) or in inconvenient temperature ranges (such as AgI). They did not stimulate widespread interest in the phenomenon of fast ion transport in solids.

Recent investigations have not, therefore, discovered a fundamentally new phenomenon, but have shown that fast ionic transport in solids is far more general than previously supposed. We now know that a broad range of cations (monovalent, bivalent, and trivalent) as well as selected monovalent and divalent anions, diffuse rapidly in certain structures.

From the scientific viewpoint, solid electrolytes are a lively subject for the solid state chemist. They are examples of a broader group of solids, which includes electronically-conductive polymers, ionically-conductive polymer membranes, and thin film inorganic solids, which challenge the chemist's creativity in understanding the chemical and physical interactions by which small changes in composition and structure can dramatically alter the macroscopic properties of a solid. The hope, of course, is that this understanding will lead to the creation of new solids and of solids in which useful properties, such as ionic conductivity, electronic conductivity, stability, and catalytic activity, are optimized.

From the technological viewpoint, high conductivity solid electrolytes have a remarkable variety of potential applications. Their initial impact was to liberate electrochemistry from the liquid state. Solid state sensors using the zirconias are already sold, as are solid state batteries for implantable medical devices. Development efforts to create new battery and fuel cell systems using solid electrolytes are active in many laboratories around the world. The challenges are formidable, and it will be a number of years before the results are clear.

The more recent discovery that lanthanide ions diffuse rapidly into the beta" aluminas has opened up an entirely new and quite unexpected direction for solid electrolyte technology. Development efforts to use solid electrolytes in opto-electronic devices have just begun.

Beyond specific materials and devices, solid electrolytes demonstrate that modern solid state chemistry can be a fascinating and lively field which includes new chemistry, fresh insights into old chemical problems, and a range of exciting materials and applications.

Bibliography

Farrington, G.C. and J.L. Briant, "Fast Ionic Transport in Solids,", *Science, 204* (1979) pp. 1371-1379.

Bates, J.B., J.-C. Wang, and M.J. Dudney, "Solid Electrolytes—The Beta Aluminas," *Physics Today, 35* (1982) pp. 46-53.

Chandra, S., *Superionic Solids: Principles and Applications*, North-Holland, Amsterdam, 1981.

Solid Electrolytes, S. Geller, ed., Springer-Verlag, New York, 1977.

Solid State Ionics—83, M. Kleitz, B. Sapoval, and Y. Chabre, eds., North-Holland, Amsterdam, 1983.

Biography

Gregory C. Farrington is Professor of Materials Science and Engineering at the University of Pennsylvania. From 1972-1979, he was a member of the research staff of the General Electric Research and Development Center in Schenectady, N.Y. Professor Farrington is the author or co-author of over 70 technical articles in the fields of electrochemistry and solid state chemistry.

MODULATED SURFACE VIBRATIONAL SPECTROSCOPIES AT ELECTRODE/ELECTROLYTE INTERFACES

By Stanley Pons, University of Utah, Salt Lake City
and
Alan Bewick, University of Southampton, Southampton, England

Introduction

Reactions at the solid-liquid and solid-gas interface have become the topic of considerable attention in the last ten years due to their controlling influence in energy-producing and catalytic devices. The complete study of these reactions can only be accomplished if something about the energetics and structure of the reactants, intermediates, and products at the interface are known, as well as the kinetic parameters. At this point, it becomes more realistic to attempt designing custom devices for specific chemical reactions. Thus in addition to being able to study the fundamental principles involved in the surface processes, there are great practical reasons to undertake these often difficult studies.

Rapid progress in this area will require collaboration between electrochemists on the one hand and materials scientists together with high vacuum surface scientists on the other. The molecular specific information now becoming available to the electrochemist from the range of techniques outlined in this article provide the vital data necessary to establish the channel of communication between the various disciplines. The electrochemist can now provide the materials scientist with the information he requires in order to model new electrocatalysts and other materials for the energy conversion area; this is one of the major immediate benefits arising from the applications of the techniques.

Some of the classically important electrochemical surface reactions which are still being intensely investigated are the redox chemistry of hydrogen at metal electrodes, metal corrosion reactions, adsorbed intermediates in the catalytic oxidation of small molecules at noble metal electrodes (fuel cells), the effects of adsorbed or chemically-bound structures on the surfaces of electrodes on the course and efficiency of solar energy conversion devices, the fundamental properties of semiconductor based energy conversion devices, and the investigation of reactions at the surfaces of battery electrodes.

In this report, we will discuss the applicability of a new infrared vibrational probe to studies of the structure and orientations of molecular species at or near the electrode-solution interface and the dynamics of adsorption/desorption processes. Such studies have been virtually impossible with available instrumentation in the past due to the extremely large absorbance by the solvent/electrolyte system. Early investigations on electrochemical systems were thus attempted primarily with internal reflectance methods that did not require that the radiation pass through the bulk solvent/electrolyte system[1] (Figure 1a). This method is limited, however, due to the few choices of infrared-transparent electrode materials (semiconducting materials or very thin metal films on insulating transparent salts and polymers) as well as more stringent cell designs and electrode geometries. In 1979, we demonstated that in fact it was possible to reflect the light externally from the electrode through the strongly absorbing solution and still obtain an infrared spectrum of very small numbers of absorbers near the electrode surface[2] (Figure 1b). This was made possible by a number of factors, including the adaptation of spectroelectrochemical potential modulation techniques that had already been developed for the ultraviolet/visible (UV/VIS) regions of the electromagnetic spectrum,[3] the use of thin layer electrochemical cells to reduce the effective path length of the strongly absorbing solution, and the development of more sensitive infrared spectrometers in our laboratories and in the commercial sector. The methods have been termed electromodulated infrared reflectance spectroscopy (EMIRS) and subtractively normalized interfacial Fourier transform infrared spectroscopy (SNIFTIRS).[4-8] Refinements to these techniques in the last five years have led to methodology which allows the study of sub-monolayer amounts of adsorbed material at electrode surfaces *in situ* to the electrochemical experiment in short periods of time. In addition, studies of chemical reactions near the surface involving electrogenerated species are also facilitated by the method, as are studies of the electrical double layer. We will present a few examples of each type of study following a brief description of the principles of infrared absorption of oscillators at metal surfaces and some details concerning the experimental apparatus and method.

Figure 1

(a) Internal and (b) external reflection spectroscopy. In (a), an evanescent wave formed at the boundary between the two media penetrates the rarer medium and can interact with absorbers close to the interface.

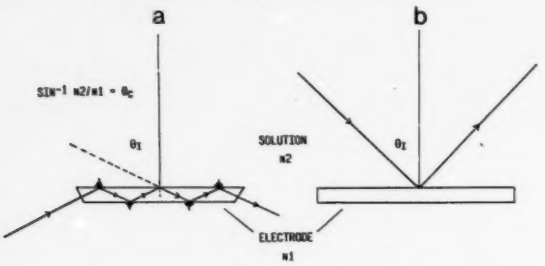

Figure 2

The relation between electric field strength, angle of incidence, and polarization of radiation with respect to the plane of incidence.

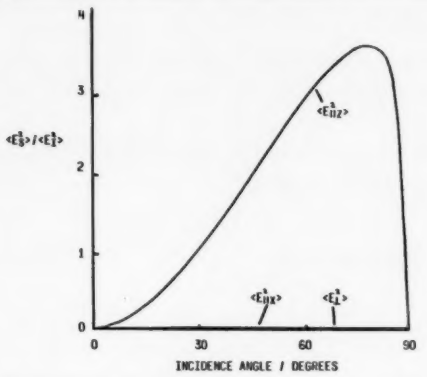

Interaction of Infrared Radiation with Adsorbed Species

The interaction of electromagnetic radiation with the surface of a highly reflecting plane metal surface depends strongly on the polarization of the radiation with respect to the incidence plane. The intensity of the electric field vector at the surface is a measure of the intensity of the radiation at the surface and is thus a measure of the energy available to interact with adsorbed oscillators at the surface. The angle of incidence of the radiation with respect to the surface also affects the field intensity of the radiation and affects the various polarizations differently. The relation between the strength of the electric field vector, the polarization of the radiation, and the angle of incidence is shown diagramatically in Figure 2. It is seen that the electric field strengths are largest at high angles of incidence to the surface normal, and that it is only the component of radiation that is polarized parallel to the incidence plane (p-polarized) that has field strength at the surface at any angle of incidence. Radiation polarized perpendicular to the incidence plane (s-polarized) is thus "blind" to absorbers present in regions very near the metal surface. Absorption of infrared radiation by a molecule occurs anytime there is an accompanying change in magnitude of an oscillating dipole moment in the molecule and a component of the electric field of the radiation that is parallel to the normal coordinate axis of that oscillating dipole. In solution, all infrared-allowd transitions will be observed at any polarization due to the radom orientation of the oscillators in the optical path. On the other hand, surface confined oscillators will have various normal coordinate dipole axes fixed with respect to the incident radiation. Since the surface also affects the magnitude of the radiation, the intensity of interaction will depend on the polarization state and the orientation of the adsorbed species. These optical properties give rise then to three important consequences to infrared spectroelectrochemistry. Firstly, s-polarized radiation is of no use in detection of species at or near the interface, and is usually eliminated by various means in the experiments described here before reaching the detector. Secondly, since none of the infrared radiation is able to give rise to a tangential field at the surface, not all of the normally infrared active vibrational modes of a molecule are observable in the adsorbed state. Those not having a finite value of $(\partial\mu/\partial Q)$ (the dipole moment derivative with respect to the normal coordinate under consideration) normal to the surface are invisible to the radiation. This is known as the vibrational surface selection rule. The magnitude of an absorption coefficient for any infrared transition is proportional to the square of the magnitude of the electric field of the radiation at the dipole and the magnitude of the dipole derivative given above. If the direction of the dipole derivative, which is a vector quantity, is tilted at some angle ϕ to the surface normal, then the intensity of the absorbance will vary as $\cos^2\phi$. Thus, the relative intensities of bands from the normal mode vibrations enable the orientation of the molecule to be deduced. Thirdly, it is also clear from the foregoing discussion that p-polarized radiation is able to interact with all species in the spectrometer optical path and all species in the reflectance cell. S-polarized radiation behaves the same except it does not interact with species close to the metal electrode surface. Thus, the difference between two beams, one p- and one s-polarized, which are of equal intensity, is simply the absorbance of those molecules near the surface; all ambient effects having been cancelled. This point is the basis for polarization modulation techniques that are also used in conjunction with the basic potential modulation schemes described herein to acquire additional information.[4-6]

In addition to the optical radiation electric field interaction with oscillating dipoles, other interactions with external electric fields are likely; we have reported observing some of these interactions recently. The perturbation of vibrational spectra by intense electromagnetic fields has been known for many years.[9-12] The effect of a strong electric field on the frequency and/or frequency splitting of a rotating molecule (the Stark effect) has been studied in the gas phase and in condensed systems.[13-17] These systems have traditionally been studied by developing the electric field with two parallel electrodes across a dielectric containing the species of interest. Also, Devlin, et. al.[18] have discussed the possibility of charge transfer interactions causing activation and perturbation of certain vibrational modes, they have discussed the participation of metal surfaces to this charge transfer mechanism. In this case, generally weaker external electromagnetic fields (crystal lattices[19], "uncharged" metal surface[20] dimers,[21] etc.) are required to cause further induced dipole effects. With regard to the former, strong interactions, Palik, et. al.[13, 14] have observed the Stark effect in several systems; but they have pointed out that the intensity changes as originally predicted by Condon[9] are the most predominant effects in the field induced infrared spectra of the systems studied. Condon pointed out that the induced dipole moment in the direction of the polarization of the electromagnetic radiation by a strong external electric field will be proportional to the square of the mean field intensity. We have observed[4, 21-24, and 34], using both EMIRS and SNIFTIRS electric field dependence in the intensity of vibrational bands that should not be active in the domain of Z-field surface selection rule predictions discussed above. We attribute these to the inducing of dipole moments by the strong electric field produced at the electrode/electrolyte solution interface; using the broadest definition, these are electrochemical manifestations of the Stark effect. In an experiment where the electromagnetic radiation is polarized in a direction ℓ, the induced dipole moment tensor in that direction by an externally applied electric field is simply:

$$P_\ell = \alpha_\ell E_\ell \qquad (1)$$

where α is the element of the polarizability tensor in the direction of the polarization of the infrared radiation, and E is the compoment of the applied electric field in the same direction. The integrated Einstein absorption coefficient for the band is given by

$$B = \frac{2\pi^2 \nu T}{\epsilon_0 hc} |P_{fi}|^2 \qquad (2)$$

where ν is the optical frequency of the infrared transition, h is Planck's constant, c is the velocity of light, T is the number of absorbing dipoles per unit cross sectional area in the radiation path, ϵ_0 is the permittivity of free space, and P_{fi} is the transition dipole matrix element. In the presence of an external magnetic field, the dipole moment tensor can be expressed in terms of the value of the permanent dipole moment and the induced value. We have shown that this leads to:[24]

$$|P_{fi}| = \langle \Psi_{\nu_f} | P_0' | \Psi_{\nu_i} \rangle + E \langle \Psi_{\nu_f} | \alpha' | \Psi_{\nu_i} \qquad (3)$$

where P_0' and α' correspond to the change in the permanent dipole moment and polarizability with respect to a normal coordinate, respectively. The integrated absorption coefficient becomes

$$B = \frac{2\pi^2 \nu T}{\epsilon_0 hc} \left| \langle \Psi_{\nu_f} | P_0' | \Psi_{\nu_i} \rangle + E \langle \Psi_{\nu_f} | \alpha' | \Psi_{\nu_i} \rangle \right|^2 \qquad (4)$$

We have calculated the expected values for the induced absorption coefficient for the C=C symmetric stretch for several molecules adsorbed flat on a metal electrode and for CO adsorbed perpendicular to the metal electrode, both in the presence and absence of an electric field. We assume close-packed simple monlayer coverage of the species on a planar 1 cm^2 surface. Since the matrix elements $\langle \Psi_{\nu_f} | a' | \Psi_{\nu_i} \rangle$ are not tabulated for molecules larger than diatomic, we have estimated the change in polarizability with normal coordinate for the given transition to be of the same order of magnitude as the fixed polarizability normal to the molecular axis. This approximation is the upper bound value of the matrix element; the actual value will normally be somewhat smaller. The results of the calculation are given in the table. These values reflect the very strong dependence of the effect on the nature of the molecule.
Examples of the effect will be discussed later in the report.

Table 1

Induced Absorption Coefficients for the C=C Symmetric Stretching Vibrations for Several Molecules and for the C=O Frequency of CO (Calculated from Equation 4) $B/10^{-3}$ cm^{-1} (Ag Mode, see text)

Electric Field Strength V/M	CO	C_2H_4	Napthalene	Anthracene	$TCNQ^-$
10^7	4.2				
10^8	4.5		0.056	0.1	1.5
10^9	7.5	0.6	5.6	11	150
2×10^9	12	2.4	22	44	580
5×10^9	30	15	140	280	3,600
8×10^9	56	40	350	710	9,300
10^{10}	79	62	560	1,100	14,500

Experimental Details

The cell for performing the EMIRS and SNIFTIRS experiments is shown in Figure 3. The working electrode is a polished mirror of the desired material and is mounted on the end of a glass syringe barrel or is attached to the end of a metal rod that is tightly sheathed in a Kel-F sleeve so that only the working face is subjected to the electrolyte solution. This assembly is fitted into a matching glass barrel which is an integral part of the cell body so that the face of the electrode is made to contact an optically transparent window at the opposite end of the cell. A thin layer of solution through which the optical beam is made to pass is thus trapped between the electrode face and the optical window. This layer is typically 1 to 100 micrometers thick, depending on the application. The cell is equipped with a Luggin capillary reference probe and a wire loop secondary electrode through which the working electrode assembly passes. The three electrode assembly allows accurate potential control to be exerted on the working electrode by conventional electrochemical potentiostat equipment. A variety of infrared optical windows may be used on the cell depending on the particular application. Polyethylene is usually used in the far-infrared region, whereas silicon, calcium fluoride, and various IRTRAN materials are common for the mid-infrared region. Flat windows are used in many cases, but prismatic types reduce reflection losses at the atmosphere/window interface allowing more of the radiation to be utilized at the solution/electrode interface. More details on the cell and experimental setup have been published.[4-6] In both EMIRS and SNIFTIRS, the cell is mounted in a spectrometer sampling area, and the radiation beam is made to reflect from the mirror electrode after passing through the solution layer. In EMIRS, the reflected beam is focussed carefully onto the entrance slit of a high-throughput infrared monochromator; and after polarization, disperson, and filtering of the radiation the beam is focussed onto the active area of a sensitive detector. The potential of the electrode is then modulated between values at which the electrochemistry is different. The population or form of the various species at the interface is also modulated at the same frequency and at the infrared radiation intensity as well. The intensity change at this modulation frequency is amplified and measured by synchronous demodulation of the detector output signal using a lock-in amplifier. This signal is stored for further processing in an integrated control computer system. The design of these high throughput instruments have been discussed elsewhere in detail.[5, 6] Presently, the EMIRS III spectrometer, is commercially available.

Further processing of the data requires normalizing the difference signal just discussed to the background throughput which is obtained by conventional chopping of the beam while scanning the spectrum. The final value may be represented as $\Delta R/R$ or the difference in reflectance at the two potentials divided by the total reflectance

Figure 3

The EMIRS/SNIFTIRS cell.

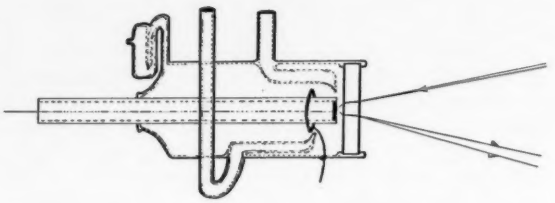

at one of the potential values. For very low values of the difference signal, the resulting ratio is equivalent to true absorbance. Due to the way in which the experiment is performed, the spectrum is of the difference type and will have bands pointing in one direction that will be due to the absorbing species at one of the potential limits and in the opposite direction for the related species at the other potential limit. The technique is highly sensitive and typically yields a noise level of only 0.00001 absorbance units through an aqueous sample in a single scan. Thus the averaging of 100 such scans gives a sensitivity of 0.000001 absorbance units which is sufficient for the study of surface coverages of much less than one monolayer.

SNIFTIRS is the equivalent technique performed on an interferometric Fourier transform infrared spectrometer. Sensitivity in this case is accomplished by the throughput and multiplex advantages of such instruments; digital signal averaging of the more intense signals at the detector allows many more spectra to be taken in unit time than the dispersive instrument. The result is similar sensitivity in both instruments if care is taken to optimize all of the relevant parameters such as throughput, detector sensitivity, cell design and alignment, etc. The choice of a suitable Fourier transform spectrometer has been discussed.[4-6] In SNIFTIRS, interferograms are recorded at each electrode potential limit individually, coadded into two separate digital files repeatedly until the required signal-to-noise level is attained, and ratioed against each other after suitable correction for radiation reflection from the front window surface. The resulting spectra are equivalent to the $\Delta R/R$ results discussed above.

Examples

There are three basic types of research that have been undertaken thus far. One has been the study of solution soluble radical ion intermediates electrogenerated at the interface from organic substrates. The thin layer cell described is ideal for the preparation of such species. In the SNIFTIRS method, spectra are first recorded at a potential value where the substrate is stable. The elec-

trode potential is then stepped to a value where all of the organic substrate in the thin layer of solution is rapidly converted to the radical ion form. Spectra are then recorded again of the interfacial area, and the two sets of data treated as described above. The second type of study has been the investigation of the structure and reorganization of the double layer region as the potential of the electrode is changed. The third line of research has concentrated on the important practical areas mentioned in the introduction: that of the structure and reactions of adsorbates at metal surfaces and the effect of surface adsorbed species on heterogeneous catalysis at electrode surfaces.

The SNIFTIRS difference spectrum of the benzophenone ketyl anion radical electrogenerated in acetonitrile at a platinum mirror electrode is shown in Figure 4. The base potential where the substrate is stable was -1.75 V and the second potential, where the radical anion is generated, was -2.50 V vs. the Ag/Ag^+ reference electrode (0.01 M to 0.2 *M* tetra-*n*-butylammonium tetrafluoroborate). The bands extending upward correspond to predominate species at the base potential (that of the substrate) while the bands extending downwards correspond to predominate species at the second potential (that of the ion radical). For reference, a conventional transmission spectrum of the benzophenone substrate is included in Figure 4. Each of the ketyl ion radical bands observed are in excellent agreement, both in frequency and intensity, with those reported by other workers. For a reversible electron transfer reaction, it can be shown that under conditions of semi-infinite linear diffusion (which should be the case in the relatively thick solution layer) the normalized reflectance should increase linearly with $\tau^{1/2}$ where τ is the electrolysis time. Using a rapid scan mode available on most Fourier transform spectrometers to obtain interferograms at 12.5 ms intervals throghout the 1.5 s duration of the pulses at the second potential, this linear relationship was verified for several of the bands in the spectrum. In this type of experiment, it is important to ensure that the thin layer contents are reproducibly returned to rest conditions after each excursion to the electrolysis potential. Thus, with reasonable care, quantitative time resolved spectrochemistry is possible using this technique.

The difference spectrum of benzophenone/benzophenone ketyl shows a large wavenumber shift in the C=0 stretching band (1661 cm^{-1} in the substrate and 1555 cm^{-1} in the ketyl anion). Strong localization of the unpaired electron at the C=0 moiety is responsible for this shift. A general red shifting of the ring modes in going from the neutral molecule to the ketyl anion was discussed previously.[25] When this same system is studied using only a very thin layer of solution (less than 1 μm), a larger percentage of the difference spectrum can be attributed to surface related phenomena. Indeed, a complex interaction is indicated by the appearance of several new bands at 1340 cm^{-1}, 1464 cm^{-1} and 2120 cm^{-}. The intensities of these bands compared to those from the anion radical in solution and the dependence upon solution thickness indicate that they are due to adsorbed intermediates probably enhanced by the Stark interactions mentioned above.

Spectra have been obtained from the potential dependent population of species in the double layer formed at a Pt electrode in contact with a simple base electrolyte in acetonitrile.[16] Figure 5 shows the potential dependence of the spectra from a 0.10 M tetrabutylammonium tetrafluoroborate (TBAF) solution of thickness about 1 μm. The base potential to which the spectra are references is -0.50 V vs. the Ag/Ag^+ 0.01 M in the same electrolyte solution. The solution was carefully dried before the measurements, and the estimated water content was less than 10^{-3} M. Marked changes are evident at the 3000 cm^{-1}, 1400 cm^{-1}, and 1100 cm^{-1} spectral regions. Figure 6 shows the same system run under the same conditions after the solution was made 0.10 in water. Additional absorbance changes are evident at the 3200-3700 cm^{-1} and the 1630 cm^{-1} regions.

Figure 4

Difference SNIFTIRS spectrum of benzophenone/ketyl radical.

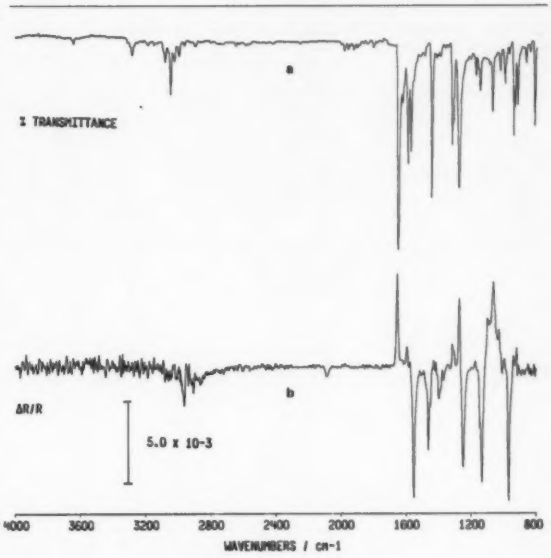

Figure 5

Difference SNIFTIRS spectrum of TBAF in dry acetonitrile.

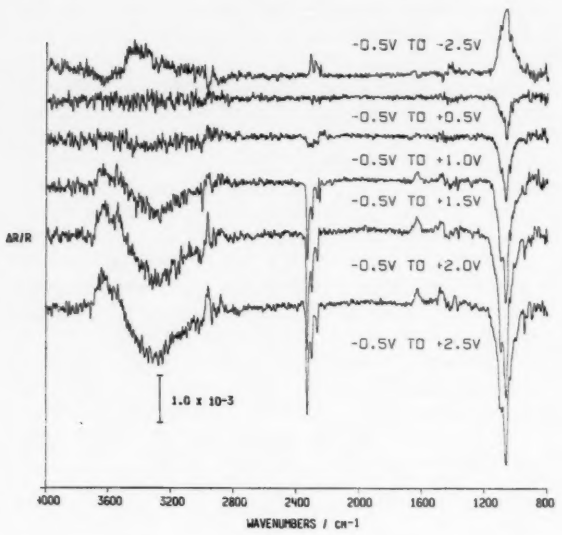

Figure 6

Difference SNIFTIRS spectrum of TBAF in wet acetonitrile.

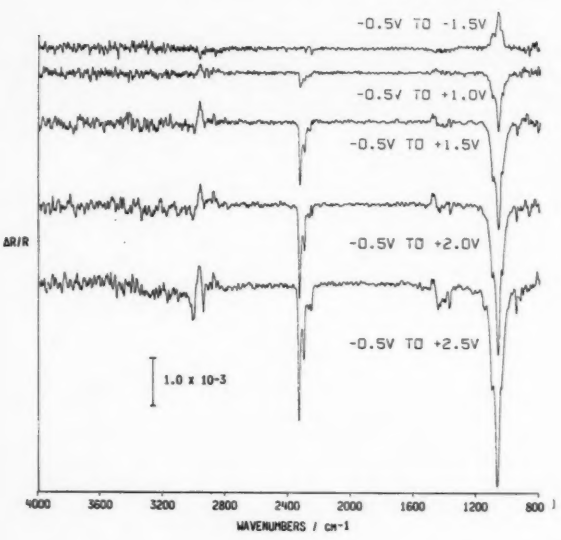

Certain aspects of the spectra are readily explained: the increasing adsorption of acetonitrile at the electrode with increasing positive potential is evident from the progressively increasing intensity at the upper potential of the 2350 cm^{-1} band. This band is strongly blue shifted from the builk acetonitrile band by the perturbation of the molecule due to adsorption (bulk acetonitrile has a C ≡ N fundamental vibrational mode at 2200 cm^{-1}). The increasing amount of anion in the double layer is indicated by the dominant downward extending bands (at high positive potentials) at 1060 cm^{-1} (tetrafluoroborate). The upward extending fine structure on the C ≡ N band between 2000 cm^{-1} and 2400 cm^{-1} is due to decreased absorption by bulk acetonitrile at the expense of adsorbed acetonitrile.

The complex structure between 3300 cm^{-1} and 3600 cm^{-1} and that near 1630 cm^{-1}, which appear when water is added to the system, can be attributed to fundamental modes of water in different environments. The broad band at 3350 cm^{-1} corresponds to extensively hydrogen bonded water, possibly associated with the anion, and it is noted that the intensity increases as more anion is drawn into the double layer. The sharper bands of opposite sign at 3625 cm^{-1}, 3550 cm^{-1}, and 1625 cm^{-1} appear to originate from water that is not so strongly perturbed by hydrogen bonding. The species responsible is probably the symmetrically bonded complex between two acetonitrile molecules and one water molecule, a species that has been well characterized previously.[27] The ν_1, ν_2, and ν_3 modes for this species are at the wavenumbers listed above. The intensities of these bands are potential dependent and are seen to decrease at the more positive potentials indicating a decreasing population of this species at these potentials.

The above assignments lead to the following general explanation of the spectra in terms of the dependence on the electrode potential of the relative amounts of each of the species in the optical path. As the electrode potential is made more positive, an increased anion concentration is required in the double layer to balance the charge. Increased amounts of acetonitrile are adsorbed at the surface as well. Increased amounts of acetonitrile are adsorbed at the surface as well. Migration of the additional anion into the optical path from the bulk electrolyte increases the total amount of anion in the path. The net increase of these two species thus accounts for the increase in intensities of the appropriate bands. As a result, bulk acetonitrile and its associated water are forced out of the region, and the intensitives are seen to be displaced in the upward direction (less absorbance) at the more positive potentials.

Changes in the C-H stretch of the cation are also observed. This band is in the 2900 cm^{-1}-3050 cm^{-1} region. The major portion of this band is extending upwards which corresponds to a net decrease in the amount of cation at the more positive potentials. Changes in

bandshape are indicated by the bands extending in the opposite direction. This example shows the considerable amount of detailed information on the composition of the double layer that becomes accessible by comparatively simple experiments. Although these first measurements have not been used to derive quantitative information on the amounts of the various species observed in the diffuse double layer or adsorbed on the electrode, it will certainly be possible to make quantitative deductions. Initially this will require careful sets of measurements on selected model systems in order to establish confidence in the calibration of band intensities for species close to or on the metal surface.

The reduction of water at metal electrodes, the hydrogen evolution reaction, and its reverse reaction, the oxidation of hydrogen, are electrocatalytic reactions with adsorbed hydrogen atoms as intermediates. On many metals, particularly those of the platinum group, there may be several kinds of hydrogen on, or partially in, the surface. On Pt and Rh electrodes, at potentials just positive of hydrogen evolution, the surface is covered by at least two types of adsorbed species. At more positive potentials, the weakly adsorbed species desorbs leaving only strongly adsorbed hydrogen. At still more positive potentials, this is also oxidized off the surface. The region of potential between that of adsorbed hydrogen and that of platinum surface oxide formation is known as the double layer region. These systems have previously been investigated by UV/visible spectroelectrochemisty.[28-29] Surface EMIRS spectra have now been obtained for Pt[30] and Rh[31] electrodes in aqueous acid solutions.

Modulation within the double layer region of potential gave only a small and featureless change of reflectivity from the electroreflectance effect and from double layer reorganization involving species not absorbing strongly in the spectral range covered.

Modulation into the potential range of strongly bound hydrogen also gave a featureless spectrum, but with a 30-fold increase in the reflectivity change, similar to the optical effect observed for this species in the UV/visible-region. It has been suggested that strongly adsorbed hydrogen consists of a proton buried just inside the metal surface with its electron in the conduction band of the metal. The increase in the number of conduction electrons on adsorption of the strongly bound species would then be responsible for the increase in reflectivity.

Modulation into the potential range weakly bound hydrogen, however, gave several absorption bands superimposed on the baseline shift from the strongly bound species also present. These bands were all at the same wavelengths as those for the vibrational modes of water, and all had the same sign, corresponding to an increase in the amount of water in the interface when weakly adsorbed hydrogen was formed. Similar experiments with H_2O/D_2O gave up to nine bands (from H_20, HDO and D_20 species) the positions of which were used to confirm the band assignment. H_20/D_20 solvent mixtures were used for two reasons. Firstly, to increase the energy transmitted through the solution in the spectral regons covering the water absorption bands and hence to increase the sensitivity in these difficult regions. Secondly, the isotopic shifts of the vibration frequencies helped with the assignment of some of the combination bands. The relative intensities of those observed bands were used to deduce the orientation of the water interacting with the weakly adsorbed hydrogen by applying the surface selection rule to a series of models. The only model which fitted the data is shown in Figure 7a. It consists of oriented dimer units bonded to hydrogen atoms on the surface, the dimer units also being hydrogen bonded to water further away from the surface. Further evidence for the strong interaction of the weakly adsorbed hydrogen with water is provided by the absence of a prominent band from the Pt-H stretch. The reference state used in determining the structure of the interacting water, which is the state of the surface in the double layer region, is also shown in Figure 7b. It is assumed to consist of a layer of water molecules, each with one lone pair orbital normal to the surface, so that the molecular dipoles are at a lower angle to the surface than is the case for the water molecules bonded to the adsorbed hydrogen. With modulating from the double layer region to the potential region of weakly adsorbed hydrogen, the water bands increase in intensity due to the surface selection rule, giving negative-going bands on adsorption. This orientation for the reference state also fits other electrochemical data.[32]

Figure 7

(a) Model of water adsorption at platinum.
(b) Assumed reference state.

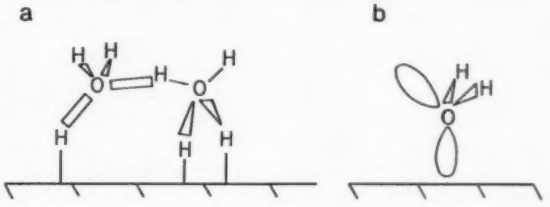

To date, fuel cells have found only limited applications in energy conversion areas in spite of their great potential benefits. The major obstacle has been the development of cheap and efficient electrocatalysts, particularly for systems directly utilizing a primary organic fuel without initial reforming. This is a prime example of an area requiring interdisciplinary collaboration of the type mentioned earlier in this article. One of the first applications of the EMIRS technique was in the detection

and identification of the major poisoning species formed on platinum group metal electrocatalysts during the electrocatalytic oxidation of fuels such as methanol, formaldehyde, or formic acid. Figure 8 gives examples of the spectra obtained from a poisoned electrode for the system platinum/formaldehyde/sulfuric acid.[33] The two bipolar bands clearly visible in Figure 8A are from the CO stretch vibrations of two different strongly adsorbed CO poisons. The higher wavenumber band is from $CO_{(ADS)}$ bonded directly on top of a surface platinum atom, and the lower wavenumber band is from the same molecular species bound in a higher coordination site between surface metal atoms. The addition of a partial monolayer of lead atoms to the surface can be seen,

Figure 8

EMIRS spectra from $Pt/HClO_4/HCHO$ system, 0 to 250 mV in (a) the absence and (b) the presence of a submonolayer amount of depostied lead.

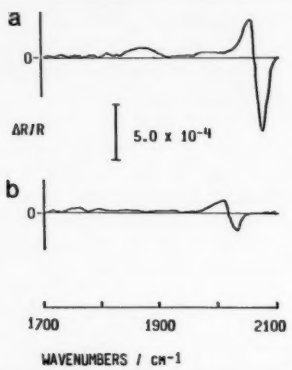

Figure 8B, to inhibit the formation of these poisons, particularly the latter, and this effect coincides with increased catalytic activity. The proper identification of the poisoning species is of considerable importance since it had been wrongly assumed from the analysis of indirect electrochemical evidence that it was $COH_{(ADS)}$. In this example, the bipolar shape of the bands arises from the considerable shift of the IR absorption bands with electrode potential for these species. This effect is in itself very interesting because of the information it gives on the nature of the bonding between the metal and $CO_{(ADS)}$.

One example of the Stark activation of a totally symmetric A_g ring mode is clearly seen in Figure 9. The experiment was by SNIFTIRS in acetonitrile solvent, from -1.5 to -2.5 V vs Ag/Ag^+ reference. The intensity (B) of the band is about 1% of the value given in the table above for an assumed field strength of 10^8 V/M. On the other hand, the upper bound value given in the table for CO predicts a 70% increase in the band intensity on going from zero field to 10^9 V M^{-1}. Since the actual effect is likely to be closer to 1% of the upper bound, we conclude that its detection will be very difficult. For ethylene, we estimate that a sensitivity of 5×10^{-5} absorbance would be required at a field strength of 10^9 V M^{-1} and thus it should be measurable. We also point out that the electrochemically activated Stark effect might be used as a probe for measuring electric field intensities in the electrical double layer. Adsorbed species will also be under the influence of a variety of fields arising from other sources such as surface adatoms, impurities, and surface defects. We also mention that the above treatment neglects quadrapole and higher expansion terms and magnetic effects, which although normally small compared to the dipole term, may be appreciable in the presence of extremely large fields. A complete vibrational analysis must include considerable of the time dependence of the electromagnetic fields of external and metal origin. Again these effects are expected to be small in the EMIRS and SNIFTIRS experiments.

Figure 9

Difference spectrum of anthracene $A_g\nu_4$ in the strong field region of a polarized electrode.

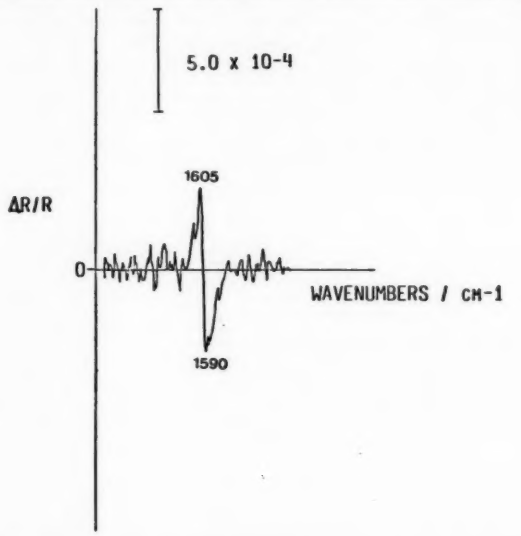

In addition to the examples, detailed studies have been undertaken on the tetracyanoethylene radical ion system, the hexacyanoferrate system, difluorobenzene adsorption, anthracene adsorption and radical ions, cyanide adsorption, the adsorption of CO and metal-CO and CO/CO interactions, small organic molecule electrocatalytic oxidations at noble metal electrodes, adsorption of nitriles, thiocyanate adsorption, and sulfate/bisulfate adsorption, and the reader is referred to other articles (reference 4-6) for a complete list of references for those studies.

Vigorous growth in EMIRS and SNIFTIRS has taken place in the last few months, and more sophisticated equipment and experiments are being planned and built. Experiments in the far infrared region (to 50 cm^{-1}) are under way presently in order to study the nature of the metal-adsorbate bond and other low frequency modes. In addition, extention of work to include single crystal electrodes has already begun; it is felt that those surfaces are required for quantitation of intensity results and a better understanding of the structure and orientation of adsorbates. Increased sensitivity of these techniques will lead to the *in situ* study of reactions and dynamics of surface reactions.

References

1. Mark, H.B. and S. Pons, *Analytical Chemistry, 38* (1966) p. 119.

2. Bewick, A., K. Kunimatsu, and S. Pons, *Electrochim. Acta, 25* (1979) p. 465.

3. McIntyre, J.E.E., *Advances in Electrochemistry and Electrochemistry Engineering Vol. 9*, R.H. Mueller, Ed., John Wiley, New York, 1973, p. 61.

4. Bewick, A. and S. Pons, *Advances in Infrared and Raman Spectroscopy*, R.J.H. Clark and R.E. Hester, Eds., Heyden and Son, London, 1985, in press.

5. Pons, S., A. Bewick, J. Russell, and J. Foley in *Modern Aspects of electrochemistry*, J.O'M. Bockris and E. Yeager, Eds., John Wiley, New York, 1985, in press.

6. Bewick, A. and S. Pons, in *Electroanalytical Chemistry*, A. Bard, Ed., Dekker, New York, 1985, in press.

7. Pons, S., T. Davidson, and A. Bewick, *Journal of Electroanalytical Chemistry, 160* (1984) 63.

8. Bewick, A., K. Kunimatsu, S. Pons, and J. Russell, *Journal of Electroanalytical Chemistry, 160* (1984) p. 47.

9. Condon, E.U., *Physics Review, 41* (1932) p. 759.

10. Crawford, M.F., H.L. Welsh, and J.L. Lock, *Physics Review, 75* (1949) p. 1607.

11. Crawford, M.F. and I.R. Dagg, *Physics Review, 91* (1953) p. 1569.

12. Crawford, M.F. and R.E. MacDonald, *Canadian Journal of Physics, 36* (1958) p. 1022.

13. Palik, E.D., R.T. Holm, A. Stella, and H.L. Hughes, *Journal Applied Physics, 54* (1982) 8454.

14. Stella, A. L. Miglio, E.D. Palik, R.T. Holm, and H.L. Hughes, *Physica, 117B, 118B* (1983) p. 777.

15. Handler, P. and D.E. Aspnes, *Physics Review Letters, 17* (1966) p. 1095.

16. Brewer, R.G. and A.D. McLean, *Physics Review Letters, 21* (1968) p. 271.

17. Sass, J.K., H. Neff, M. Moskovits, and S. Hollway, *Journal Physical Chemistry, 85* (1981) p. 621.

18. Devlin, J.P. and K. Consani, *Journal Physical Chemistry, 85* (1981) p. 2597.

19. hester, R.E., *Advances in Infrared and Raman Spectroscopy*, Vol. 4, R.J.H. Clark and R.E. Hester, Ed., Heyden and Son, London, 1978, Chapter 1.

20. Lehwald, S. H. Ibach, and J.E. Demuth, *Surface Science, 78* (1978) p. 577.

21. Pons, S., S.B. Khoo, A. Bewick, M. Datta, J.J. Smith, S. Hinman, and G. Zachmann, *Journal Physical Chemistry* (1984).

22. Pons, S. and A. Bewick, *Langmuir*, in press.

23. Bewick, A. C. Gibilaro and S. Pons, *Langmuir*, in press.

24. Bewick, A. S. Pons, and C. Korzeniewski, *Electrochimica Acta*, in press.

25. Aleksandrov, I.V., Y.S. Bobovich, V.G. Maslovad, and A.N. Siderov, *Optical Spectroscopy 35* (1973) p. 154.

26. Pons, S., T. Davidson, and A. Bewick, *Journal of Electroanalytical Chemsitry, 140* (1982) p. 211.

27. Saumagne, P., Ph.D. Thesis, Universite de Bordeaux, Frnace, 1981.

28. Bewick, A. and A.M. Tuxford, *Journal of Electroanalytical Chemistry, 47* (1973) p. 253. A. Bewick, K. Kunimatsu, J. Robinson and J.W. Russell, *Journal of electroanalytical Chemistry, 119* (1981) p. 175.

29. McIntyre, J.D.E. and W.F. Peck, *Proceedings Symposium Electrocatalysis*, The Electrochemical Society, San Francisco, 1974.

30. Bewick, A. and J.W. Russell, *Journal of Electroanalytical Chemistry, 132* (1982) p. 329.

31. Bewick, A. and J.W. Russell, *Journal of Electroanalytical Chemistry, 142* (1982) p. 337.

32. Trasatti, S., *Journal of Electroanalytical Chemistry*, in press.

33. Bewick, A., Symposium on the Chemistry and Physics of Electrocatalysis, *The Electrochemical Society*, San Francisco, (1983).

34. Bewick, A., *Journal of Electroanalytical Chemistry, 150* (1983) p. 481.

Biography

Dr. Stanley Pons is Associate Professor of Chemistry at the University of Utah and is a principal investigator for the Office of Naval Research in electrochemistry. His research has been in the areas of spectroelectrochemistry, ultramicroelectrodes, reaction mechanisms, and catalysis. Proessor Alan Bewick is a Reader in Chemistry at the University of Southampton, England. His research has been primarily in spectroelectrochemistry, the chemistry and physics of clean surfaces, and electrocatalysis. The two authors were the first to demonstrate the utility of infrared spectroscopy in the study of reactions at the electrode—solution interface.

DEPARTMENT OF THE NAVY
OFFICE OF NAVAL RESEARCH
ARLINGTON, VA. 22217

OFFICIAL BUSINESS
PENALTY FOR PRIVATE USE, $300

THIRD-CLASS MAIL
POSTAGE & FEES PAID
USN
PERMIT No. GS-9

For sale by the Superintendent of Documents, U.S. Government Printing Office
Washington, D.C. 20402